

*Fachbereiches C - Physik*  
*Universität Wuppertal*

**Simulations for Radio Detection with Auger**

***MASTER THESIS***

**Li Feng**

*March 2010*



# Contents

<b>1. Introduction</b>	<b>1</b>
<b>2. Physics of Ultra High Energy Cosmic Rays</b>	<b>3</b>
2.1. Energy spectrum . . . . .	3
2.2. Chemical Composition . . . . .	5
2.3. Origin . . . . .	6
2.4. Propagation . . . . .	8
2.4.1. Effects of the magnetic fields . . . . .	8
2.4.2. Energy losses and GZK process . . . . .	8
<b>3. Cosmic Ray Induced Air Showers</b>	<b>11</b>
3.1. Air Shower Development . . . . .	11
3.1.1. Hadronic component . . . . .	12
3.1.2. Electromagnetic component . . . . .	12
3.1.3. Muonic component . . . . .	13
3.2. The longitudinal Shower-Profile . . . . .	13
3.3. The Shower Footprint on Ground . . . . .	16
<b>4. Simulation of Air Shower</b>	<b>19</b>
4.1. Introduction to CORSIKA . . . . .	19
4.2. Program model options . . . . .	20
4.3. Data Files . . . . .	22
4.3.1. Input Files . . . . .	22
4.3.2. Output Files . . . . .	23
<b>5. Simulation of Radio Emission</b>	<b>25</b>
5.1. Geosynchrotron Model . . . . .	25
5.1.1. Synchrotron-theory: individual particles . . . . .	25
5.1.2. Synchrotron-theory: electron-positron pairs . . . . .	27
5.2. Introduction to REAS . . . . .	28
5.3. Data Files . . . . .	29
5.3.1. Input Files . . . . .	29
5.3.2. Output Files . . . . .	30
<b>6. Simulation Result</b>	<b>31</b>
6.1. Introduction . . . . .	31
6.2. Simulation parameters . . . . .	31

*Contents*

6.3. Consumption Time . . . . .	31
6.4. Radial dependence and emission pattern . . . . .	34
6.5. Zenith dependence and emission pattern . . . . .	35
6.6. Shower azimuth angle . . . . .	36
6.7. Maxium/Integral ratio . . . . .	40
6.8. Symmetry N-S and E-W . . . . .	42
6.9. Conclusions . . . . .	45
<b>7. Summary and Outlook</b>	<b>47</b>
<b>8. Acknowledgement</b>	<b>49</b>
<b>A. Input Card Example</b>	<b>51</b>
<b>B. REAS Parameter File Example</b>	<b>53</b>
<b>C. Example of raw data from REAS2</b>	<b>57</b>

# 1. Introduction

The nature of the ultra-high-energy cosmic rays (UHECRs) remains one of the fundamental questions we want to find out, Since Viktor Hess discovered the existence of cosmic rays in the early 20th century. Charged particles with energies ranging from a few times  $10^6$  up to  $> 10^{20}$  eV, continuously impinge on the earth as so-called “cosmic rays” , which corresponds to the energy of a well hit tennisball carried by a single particle at maximum. When a primary cosmic ray enters the atmosphere, an extensive cascade of ionized particles and electromagnetic radiation would be produced, which we called an extensive air shower.

As it is first discovered in mid-1960, cosmic ray air showers have been known to emit pulsed radio emission in the frequency range from a few to a few hundred MHz. Now, people make effort to study the radio emission from the extensive air shower. For instance, digital “software radio telescopes” such as LOFAR and the particle detector array such as Pierre Auger Observatory are working in process.



## 2. Physics of Ultra High Energy Cosmic Rays

In 1922, Austrian physicist Victor Hess showed the famous balloon experiment, that he measured the radiation at different altitude. As it is expected, at the height of 1000 m, the ionization decreased. But after reaching a higher height of 3000 m, the ionization is as strong as it is on the Earth surface. He concluded, that the cause of that boost in ionization might be attributed to the penetration of the Earth atmosphere from outer space by hitherto unknown radiation of high penetrating capacity[1]. The systematic study of reactions induced by cosmic radiation, lead to the discovery of the protons, helium, carbon, nitrogen and other heavy ions up to iron[2].

During the 1930s, a wide variety of experimental investigations demonstrated that the primary cosmic rays are mostly positively charged particles. From the 1930s to the 1950s, before man-made particle accelerators reached very high energies, cosmic rays served as a source of particles for high energy physics investigations, and led to the discovery of subatomic particles that included the positron and muon. The existence of events above  $10^{20}$  eV has been established in different experiments since the first observation by Linsley in his pioneering work of 1966 [3].

As well as these applications continue, the cosmic ray research has been directed towards astrophysical investigations of the origin of cosmic rays, such as, wherer does they come from of the Galaxy, how they get accelerated to such high energies, and what their composition tells us about matter from outside the solar system.

### 2.1. Energy spectrum

In order to understand the origin and nature of the highest energy cosmic rays, the analysis of their overall energy spectrum has began. As it is shown in 2.1, that compares the differential all-particle spectrum.

Obviously, the spectrum can be approximated by an inverse power law in energy with an differential flux given by

$$\frac{dN}{dE} \propto E^{-\alpha}, \text{ with } \alpha \sim \begin{cases} 2.7 & : E < 4 \cdot 10^{15} \text{eV} \\ 3.0 - 3.1 & : 4 \cdot 10^{15} \text{eV} \leq E \leq 3 \cdot 10^{19} \text{eV} \\ 2.7 - 3.0 & : E \geq 3 \cdot 10^{19} \text{eV} \end{cases}$$

## 2. Physics of Ultra High Energy Cosmic Rays

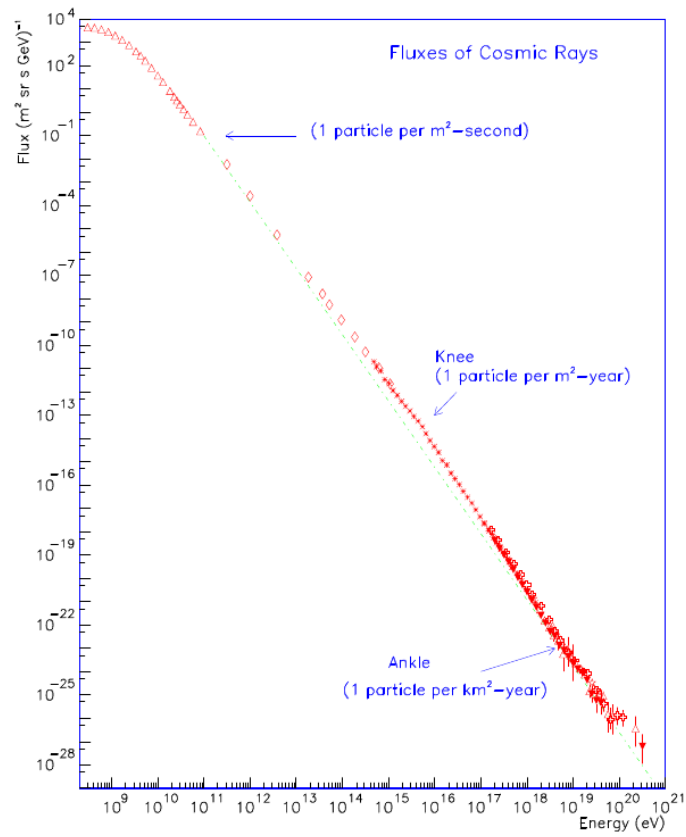


Figure 2.1.: Differential energy spectrum of the Ultra-High-Energy Cosmic Rays [13]

At low energies the index  $\alpha$  is about  $2.6 \sim 2.7$ . At energies around  $3 \cdot 10^{15}$  the first feature, then so called *knee*, shows up with a steepening of the spectrum described by an index  $\sim 3$ . A further steepening, the *secondknee*, at an energy of  $\sim 5 \cdot 10^{17}$  eV, with index  $\sim 3.3$  is reported in [4, 5]. At energies of  $\sim 10^{19}$  eV, the so called *ankle*, a very pronounced flattening, with index  $\sim 2.7$ , appears [6].

## 2.2. Chemical Composition

As it is shown in 2.2, compared with the composition of the stellar material in our solar system, the chemical composition of cosmic rays does not have too much difference. However, we need to be concerned about some differences, which are very important. Obviously, Lithium, Beryllium and Boron are overabundant in cosmic rays. Meanwhile, there is an overabundance of Hydrogen and Helium for solar system abundances.

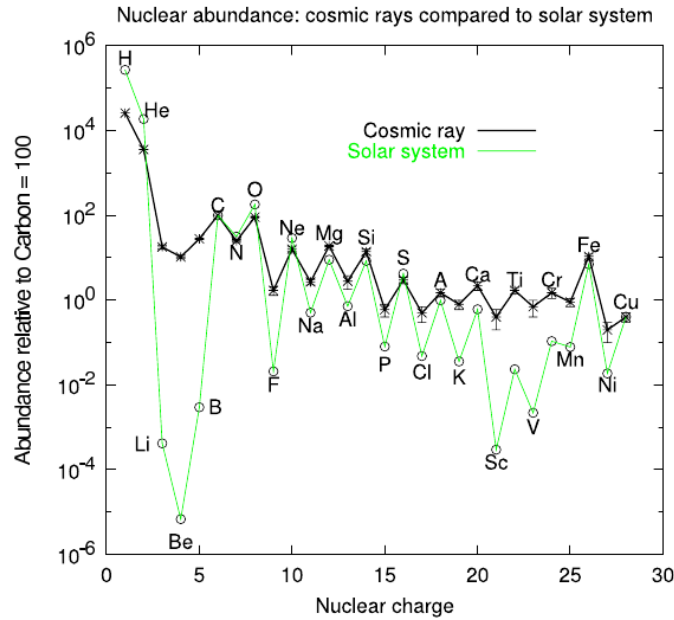


Figure 2.2.: The abundances of various nuclei in the cosmic radiation compared to the abundances in the solar system, From [14].

To characterize the cosmic-ray mass composition one uses commonly the mean logarithmic mass  $\ln A$ , defined as

$$\ln A = \sum r_i \ln A_i, \quad (2.2)$$

where  $r_i$  is the relative fraction of nuclei with atomic mass number  $A_i$ .

The mean logarithmic mass from experiments measuring electrons, muons, and hadrons at ground level using mostly CORSIKA/QGSJET to interpret the data are compiled in [3]. The standard interpretation for the ankle is that the flat extragalactic component

## 2. Physics of Ultra High Energy Cosmic Rays

crosses the steep Galactic spectrum, generating this feature just above the intersection energies[16]. The spectrum of the extragalactic component is consistent with the slope originating from acceleration in strong or ultra relativistic shocks. To explain a predominantly heavy composition up to  $10^{15}$  eV, a model invoking an extragalactic component with mixed composition could be a favored solution. Based on the predictions reported in [7], the pair production dip model has been very proposed recently [8]. Assuming an extragalactic proton component, the dip is obtained naturally from the interaction with the cosmic microwave background ( $e^+e^-$  pair production). At around  $10^{18}$  eV (second knee), the transition to the extragalactic component is expected to occur, and proton dominated in the composition in this range.

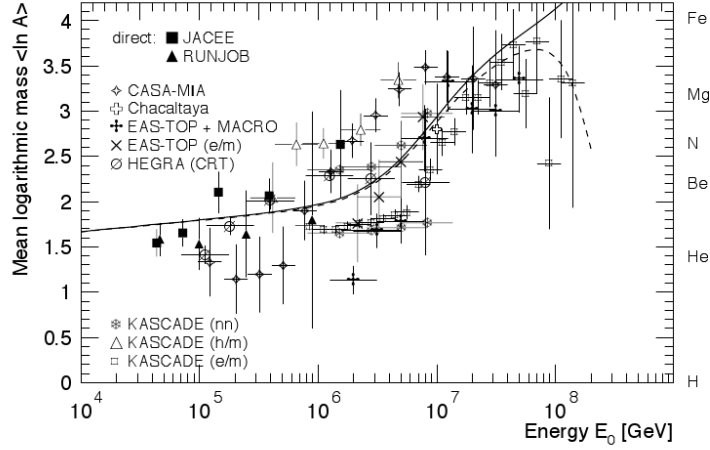


Figure 2.3.: Mean logarithmic mass  $\langle \ln A_i \rangle$  as a function of Energy, measuring electron, muons and hadrons at ground level. Modified from[15]

### 2.3. Origin

The most favorite acceleration mechanisms are based on a model by Enrico Fermi. He proposed that charged particles gain their energy by a statistical acceleration due to multiple scattering in turbulent magnetic fields. These fields might occur when a plasma shockwave propagates into the interstellar medium as observed at supernova explosions. Traversing through the shock front, the particle will gain an energy  $\frac{\Delta E}{E} \sim \beta^\alpha$ , where  $\beta = \frac{v}{c}$  is the speed of the plasma and  $\alpha$  a model dependent parameter. However, this mechanism will only work as long as the particle is trapped within the accelerating area. The Larmor radius  $r_L$  of a particle with the charge  $Z$  gyrating in a magnetic field  $B$  is:

$$r_L \propto \frac{E}{Z \cdot B} \quad (2.3)$$

As soon as the Lamor radius exceeds the extend of the source  $L$ , the particle will leave the area and the acceleration is stopped. The maximum energy that can thus be obtained is governed by the size and the magnetic field strength  $B$  of the accelerator. This has been summarized by A.M. Hillas [9] in the following constraint on the maximum energy  $E$ :

$$E_{15} < \frac{1}{2} B_{\mu G} \cdot L_{pc} \cdot \beta \cdot Z \quad (2.4)$$

With respect to the highest energies of  $10^{20}$  eV, [?] shows possible accelerators due to their size and magnetic field strength. Objects that lie below the diagonal do not fulfill the condition of eqn 2.4. The solid line restricts the candidates for  $10^{20}$  eV protons and the dashed line for  $10^{20}$  eV iron nuclei, which can be accelerated more easily due to their higher atomic numbers. While these two lines refer to a maximum velocity of the accelerating shock front of  $v \approx c$ , a more realistic assumption of the speed of plasma with  $\sim 1000$  km will lie within the shaded area. Consequently only 4 feasible candidates remain: Neutron stars, active galactic nuclei (AGNs), radio galaxy lobes and clouds of intergalactic matter.

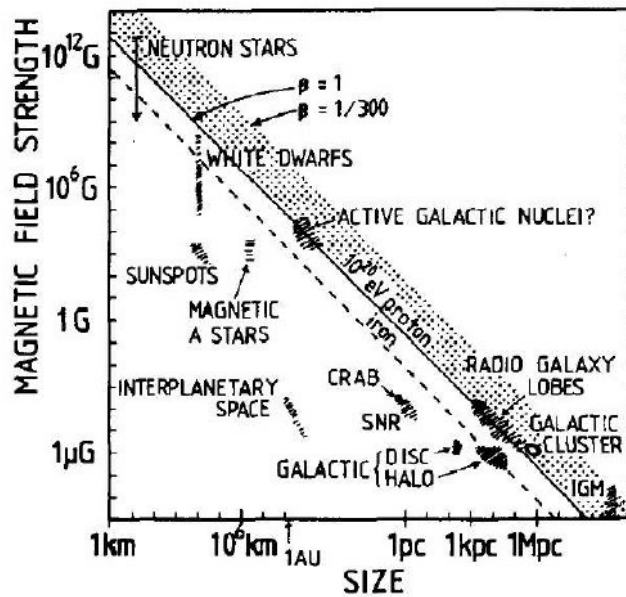


Figure 2.4.: The Hillas Plot regarding sources of cosmic rays due to their extend in Mpc and magnetic field strength in Gauss[16].

However, for the propagation of the ultra-high-energy cosmic rays above  $10^{18}$  eV further effects come into play.

## 2.4. Propagation

### 2.4.1. Effects of the magnetic fields

In their journey from their sources to the Earth, cosmic rays are deflected by magnetic fields. A regular intergalactic field, the value of which is lower than  $10^{-9}$  G, is strongly constrained to by rotation measures of extra-galactic radio sources. Galaxy clusters may have stronger magnetic fields, coherent over Mpc scales.

The magnetic field in our Galaxy is known to have a regular large scale structure. The typical value of the galactic magnetic field is a few  $\mu G$ , approximately uniform over scales of the order of a few kpc. The magnetic field lines follow the spiral arms. Different models are built depending on the sign of the field in the arms and on the symmetry with respect to the galactic plane.

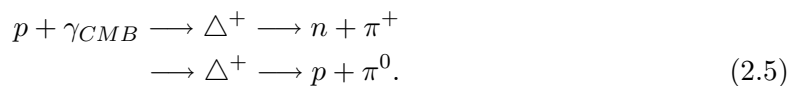
Fig 2.5 depicts trajectories of nuclei with  $E/Z = 1$  and 10 EeV in the BSS-S galactic magnetic field model, that we will take as the reference one to illustrate most of the effects discussed in this work. When  $E/Z = 1$  EeV the nuclei follow helical trajectories that make a very large number of turns before their arrival to the Earth. These highly twisted paths are not exclusive of finely tuned, isolated incoming directions, but rather are a typical feature at these energies. Notice that the direction of entrance to the Galaxy need not be close to the disk in order for the UHECR to get trapped along the spiral structure of the magnetic field (dashed lines). When  $E/Z = 10$  EeV the CRs follow instead much straighter paths.

The gyro-radius, for a proton at 1 EeV in a field of  $\sim 3 \mu G$  is about 300 pc, namely the thickness of the Galactic disc. The motion of nuclei with rigidity  $E/Z$  above 10 EeV is instead not significantly affected by the magnetic field since the gyro-radius for a particle of that energy is of the same order as the traveled distance. In this case the information on the incoming direction is conserved and the correlation with sources can in principle be established. The key quantity to determine the angular deflection from the incoming cosmic ray path, as a function of the traveled distance and primary energy, is the particle Larmor radius,  $r_L \simeq E/(Z \cdot B_{\perp})$ . Where  $Z$  is the charge of the particle and  $B_{\perp}$  is the magnetic field component perpendicular to the particle momentum.

### 2.4.2. Energy losses and GZK process

After the discovery of the cosmic microwave background (CMB), it is predicted that, due to photopion production on the CMB, the spectrum of cosmic rays protons would show a cutoff at about  $5 \cdot 10^{19}$  eV, which has become known as the GZK-cutoff.

Ultra-high-energies interact with the 2.7 K cosmic microwave background, when they transverse the intergalactic space. The main involved processes for protons in this energy range are the following:



In the laboratory frame, the center of momentum energy squared is:

$$s = m_p^2 + 2E_p\epsilon(1 - \beta \cos \theta) \quad (2.6)$$

where  $\epsilon$  is the energy of the photon and  $\beta$  is the proton speed ( $c = 1$ ).

The threshold energy for a proton to produce a pion on the photons of CMB in a head-on collision is:

$$E_{th} = \frac{m_\pi}{4\epsilon}(2m_p + m_\pi) \simeq 6.8 \cdot 10^{16} \left(\frac{\epsilon}{\text{eV}}\right)^{-1}$$

eV, (2.7) which, dealing with average photon energies of  $\sim 6 \cdot 10^{-4}$  eV, leads to  $\sim 10^{20}$  eV, but can be smaller since the microwave spectrum extends to higher energies ( $\sim 10^{-3}$  eV). The energy dependence of the mean free path of the proton is:

$$\frac{1}{\lambda_p \gamma} = \frac{1}{8\beta E_p^2} \int_{\epsilon_{th}}^{\infty} \frac{n(\epsilon)}{\epsilon^2} d\epsilon \int_{s_{min}}^{s_{max}} (s - m_p^2) \sigma_{p\gamma}(s), \quad (2.8)$$

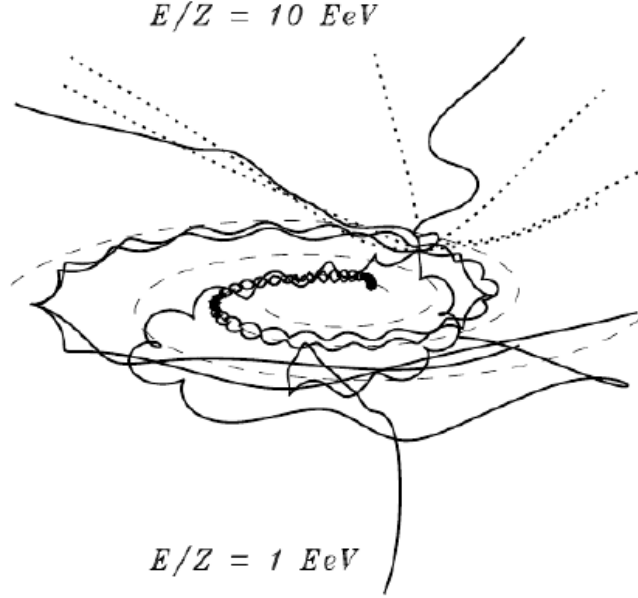


Figure 2.5.: Examples of trajectories of nuclei with  $E/Z = 1$  EeV (solid lines) and 10 EeV (dotted lines) in the galactic magnetic fields (BSS-S model). From [17]

where  $n(\epsilon)$  is the photon number density per energy,  $s_{min}$  and  $s_{max}$  are the squares of minimum and maximum energies in the center of mass system. The mean free path for a proton can be estimated as  $\approx 8$  Mpc, where  $n \approx 400 \text{ cm}^{-3}$  is the CMB photon density, and  $\sigma_{p\gamma} \approx 10^{-28} \text{ cm}^{-2}$  is the process cross section at the threshold energy. The neutron decay length is about 1 Mpc at  $10^{20}$  eV, so that on these length scales it decays before interacting.



## 3. Cosmic Ray Induced Air Showers

When cosmic rays enter the earth atmosphere they will collide with nucleus of the air and produce secondary particles, which will collide with air nuclei and thus a cascade of secondary particles are formed. The number of generated particles at first multiplies, then reaches a maximum before it attenuates more and more as particles fall below the threshold for further particle production. In this particle cascade, hadronic and electromagnetic interactions as well as particle decays take place forming a disc of different particles. This is what we called the air shower.

Air Shower was first discovered by the French physicist Pierre Auger, he and his colleges could show the existence of air showers with the coincidence studies with counters and Wilson chambers partly at sea level and partly in two high altitude laboratories, Jungfrauoch (3500 m) and Pic du Midi (2900 m)[10]. With the two parallel and horizontal counters, they searched for coincidences and concluded the existence of primary particles with energies around  $10^{15}$  eV. Nuclear cascades are initiated by cosmic rays of very high energy and many of the products reach the ground before losing all their energy. From then on, the understanding of the physics of air showers has reached a fairly detailed level. The consequential attenuation of the cosmic ray flux at the highest energies has recently been observed above  $10^{19.5}$  eV by the Pierre Auger Observatory [12].

### 3.1. Air Shower Development

The first interaction of the primary cosmic ray with the atmosphere typically occurs at a height of 20-30 km, depending on the energy and mass of the primary particle. Assuming a primary cosmic ray nucleon, mostly kaons and muons together with a leading baryon are produced sharing the primary energy. Due to the large primary energy these secondary particles can again interact with other nuclei and produce new particles.

When a primary particle enters the Earth atmosphere, an air shower starts to develop. Usually, the first interaction is an inelastic nuclear collision producing several secondary particles, and they also produce secondaries similar to their predecessors. Usually one distinguishes three different components of the cascade, connected to different interaction processes (as sketched in 3.1):

- Hadronic component
- Muonic component

### 3. Cosmic Ray Induced Air Showers

- Electromagnetic component

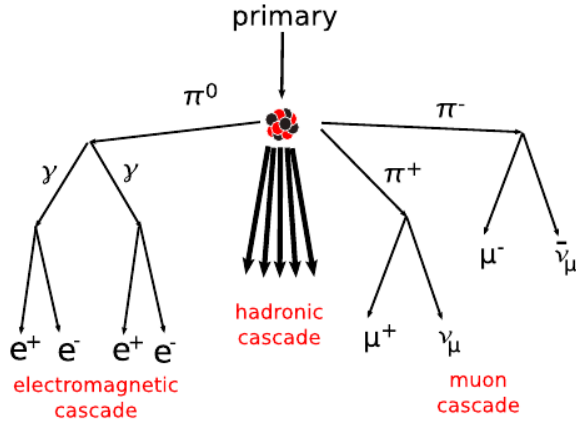


Figure 3.1.: Three main components of extensive air showers [18].

In the next section, these three different components of the cascade will be introduced.

#### 3.1.1. Hadronic component

The pions or other mesons, and three quark composed particles, baryons consist about 1% of all particles detected at ground level, and represent the hadronic component of the EAS. The first collision typically produces more than fifty secondaries and they carry most of the energy in the early shower stage. They are emitted closely to the original particle direction with their high longitudinal momentum. And their lateral spread is only a few tens of meters at observation level. Fluctuation in the hadronic component can significantly influence the development of the other two components as they evolve from it.

#### 3.1.2. Electromagnetic component

The electromagnetic component of a hadron induced EAS essentially originates from the decay of neutral mesons, mainly pions:

$$\begin{aligned} \pi^0 &\longrightarrow \gamma + \gamma (\sim 98.8\%) \\ &\longrightarrow \gamma + e^+ + e^- (\sim 1.2\%). \end{aligned} \quad (3.1)$$

Electromagnetic cascades can also be initiated directly by high energy photons or electrons. During an interplay between pair production and bremsstrahlung an electromagnetic cascade can develop. In an electromagnetic field of a nucleus  $N$  the pair production

process can be described as

$$\gamma + N \longrightarrow N + e^- + e^+, \quad (3.2)$$

whereas bremsstrahlung leads to

$$e^\pm + N \longrightarrow N + e^\pm + \gamma, \quad (3.3)$$

The emission of further photons may produce additional  $e^\pm$  pairs. This reaction chain proceeds until a threshold energy (critical energy)  $E_c = 85.1$  MeV in air is reached. For  $E < E_c$  the ionization energy loss starts to dominate the bremsstrahlung process and the electron is attenuated within one radiation length.

### 3.1.3. Muonic component

The muonic component of an EAS emerges from the decay of secondary pions and kaons of the hadronic component:

$$\begin{aligned} \pi^\pm &\longrightarrow \mu^\pm + \nu_\mu(\bar{\nu}_\mu) (\sim 99.99\%) \\ K^\pm &\longrightarrow \mu^\pm + \nu_\mu(\bar{\nu}_\mu) (\sim 63.51\%) \end{aligned} \quad (3.4)$$

Indeed, the daughter muons are also unstable with typical lifetimes of  $\tau_\mu \sim 2.2 \mu\text{s}$ . If taken their experienced time dilatation into account, most of them reach the ground, except the particles with energy smaller than a few GeV. Therefore, the muonic component is also called the hard component of cosmic radiation. Muons are not much deflected by multiple scattering on their way to the ground. Their path through the atmosphere is almost rectilinear and makes detection on the ground very helpful for reconstructing the early stage of the shower development. The highest energy muons result from high energy pions and kaons. Thus they carry important information about the hadronic interaction at those energies which can be used to test theoretical interaction models. Studying high energy muons near the shower core therefore yields information about the nature of the primary particle.

## 3.2. The longitudinal Shower-Profile

The longitudinal shower profile describes the number of particles  $N(X)$  as function of the atmospheric depth  $X$ . The longitudinal evolution of the shower is dominated by the electromagnetic cascade. The number of particles increases with the shower depth and reaches its maximum at a characteristic depth  $X_{max}$ . And the electromagnetic component starts to attenuate. The total integrated energy deposit is a good calorimetric measure, while  $X_{max}$  is a measure of the primary particle mass. The mass dependency of  $X_{max}$  for a fix energy can be understood in terms of the so called superposition model.

### 3. Cosmic Ray Induced Air Showers

Here, a primary of mass  $A$  and energy  $E$  is considered as bunch of  $A$  independent protons of the energy  $E/A$ . One would expect that in the average this shower profile reaches its maximum higher in the atmosphere as a proton induced shower of energy  $E$ . More quantitatively, the shower development can be investigated by the Heitler model [11]. This toy model neglects multiple scattering and Compton scattering effects and characterises the electromagnetic shower development by bremsstrahlung and pair production. It is assumed that the photon energy in pair processes is shared between both leptons. Furthermore, the energy of an electron in a bremsstrahlungs-processes is shared between the photon and outgoing electron. A scheme of this procedure is shown in 3.2.

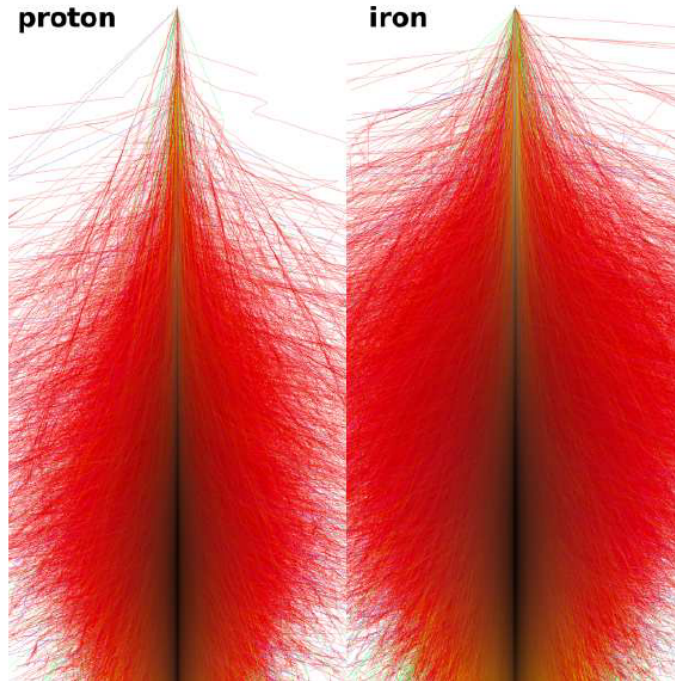


Figure 3.2.: The longitudinal shower development for a 1015 eV vertical proton and iron induced shower simulated with CORSIKA. From [19].

An electron is supposed to emit a photon after travelling a splitting length  $d = \ln 2 X_0$ , where  $X_0$  is the radiation length of air. This photon produces a  $e^+e^-$  pair after travelling another  $d$ . Thus, the shower expands like a tree, that bifurcates every grammage  $d$ . Therefore, the number of particles at a certain depth is

$$N(X) = 2^{d/X_0}.$$

(3.5)

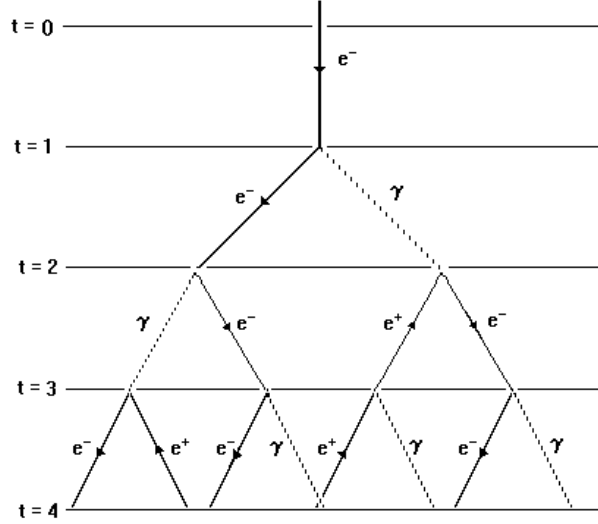


Figure 3.3.: A schematic sketch of the Heitler formalism for the electromagnetic cascade.

The average energy per particle is assumed to be

$$E(X) = \frac{E_0}{N(X)}. \quad (3.6)$$

This bifurcation continues until the critical energy is reached. Therefore

$$X_{max} = X_0 \ln(E_0/E_C). \quad (3.7)$$

Reasoning with the superposition principle, the following trend becomes obvious:

$$X_{max} \propto \ln(E_0/A). \quad (3.8)$$

The dependence on  $A$  demonstrates that on average showers generated by heavy primaries develop more rapidly than proton showers with the same energy. Unfortunately,

### 3. Cosmic Ray Induced Air Showers

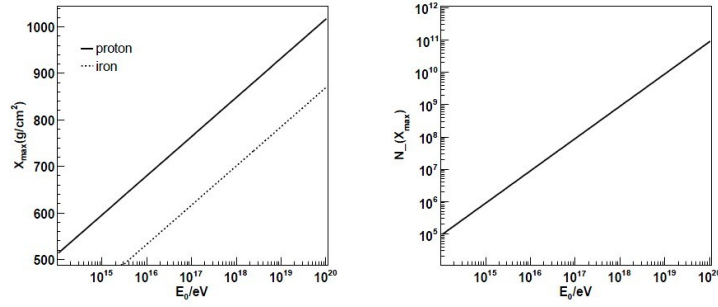


Figure 3.4.: From left to right are the  $X_{max}$  and  $N_{max}$  Predictions for a pure electromagnetic cascade in the Heitler toy model. [18]

there is only a logarithmic dependency on the mass, which makes it difficult to distinguish between masses.

Another distinguishing feature is the fluctuations in their longitudinal development. Heavy nucleons tend to have smaller fluctuations since each nucleus can be described as a beam of many incident nucleons.

### 3.3. The Shower Footprint on Ground

While propagating through the atmosphere the shower-front evolves conically around the primary trajectory. This is known as leading particle effect and allows to track the primary. The particle density in the perpendicular plane of the shower-axis is expected to be radial symmetric and steeply falls with the distance from the shower impact point. The lateral density at a predefined distance can be used as measure for the primary energy. If it is possible to distinguish between the muonic and electromagnetic component of the particles at ground this information can be used to unfold the primary mass compositions of the showers.

At ground, the shower front consists mostly of photons, electrons and muons. The majority of relativistic hadrons is concentrated around the core and can be neglected 50 m away. Usually, the soft component thins out and the electrons arriving on ground have much lower energies than the muons. The most dominant energy loss is due to bremsstrahlung. The interaction cross-section scales with  $m^{-4}$ . Therefore, the heavy muons can penetrate much deeper into the atmosphere than electrons 3.5.

Therefore, muons are also called the hard component of a shower. For low energy primaries only the hard component reaches ground. The electromagnetic and hadronic component is also referred to as soft component of a cascade as these particles tend to deposit far more energy per atmospheric depth than the muons and neutrinos. Thus, from the footprint one can distinguish a young shower with a electron dominated shower-

### *3.3. The Shower Footprint on Ground*

front far away from the core and an old shower, that shows a muon dominated component far away.

### 3. Cosmic Ray Induced Air Showers

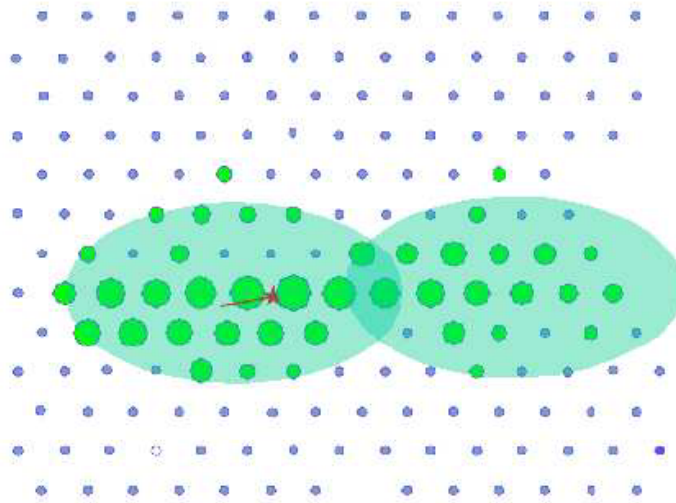


Figure 3.5.: The muonic component travels, especially in horizontal showers, and make a separation of the positive and negative charged muons visible in the footprint.

## 4. Simulation of Air Shower

Ultra High Energy Cosmic Rays, especially those energies over  $10^{20}$  eV have been observed are inadequate. And at the same time, Large Hadron Collider (LHC) [22], the world's largest and highest-energy particle accelerator ever, intended to collide opposing particle beams of either protons at an energy of 7 TeV per particle, or lead nuclei at an energy of 574 TeV ( $0.5 \cdot 10^{15}$ ) per nucleus. Obviously, Nature is able to produce single particle energies much larger than what we can produce artificially. Nevertheless, people find other ways to work over. Simulation study is one method that widely used in this field. Therefore, a number of computer programs has been written to simulate the development of EAS in the atmosphere and a considerable number of publications exists discussing the results of such calculations.

Monte Carlo methods are widely used classes of computational algorithms for simulating the behavior of various physical and mathematical systems. They are distinguished from other simulation methods by being stochastic usually by using random numbers. A detailed Monte Carlo program would be a good tool to study the evolution and properties of extensive air showers in the atmosphere.

In order to simulate the radio emission we need, which for the purpose of this work is the actual signal, protons and heavier nuclei are generated at the top of the atmosphere and propagated down to the Earth surface using the air shower generator CORSIKA. In this chapter, detailed information about CORSIKA will be introduced.

### 4.1. Introduction to CORSIKA

Most of our understanding of the evolution and properties of air showers come from detailed studies made with Monte Carlo simulations. CORSIKA (COsmic Ray SIMulation for Kascade)[21] is a detailed Monte Carlo program to study the air shower in the atmosphere. It is originally developed to perform simulations for the Kascade experiment [23] at Karlsruhe in Germany. But during the time it became a tool that is used by many groups. Its applications range from Cherenkov telescope experiments ( $E_0 \sim 10^{12}$  eV) up to giant cosmic ray surface experiments at the highest energies observed ( $E_0 > 10^{20}$  eV).

CORSIKA allows to simulate the interactions and decays of nuclei, hadrons, muons and photons in the atmosphere up to energies of some  $10^{20}$  eV. These particles are tracked through the atmosphere until they undergo reactions with the nuclei in the air. The program gives type, energy, location, direction and arrival times of all secondary particles that are created in the air shower and pass a selected observation level.

The CORSIKA program is a complete set of standard FORTRAN routines and consists

## 4. Simulation of Air Shower

basically four parts:

- The first part handles the input and output, performing decay of unstable particles and tracking of the particles taking into account ionization energy loss.
- The second part treats the hadronic reactions of hadrons with air nuclei at higher energies.
- The third part simulates the hadronic interactions at lower energy.
- The fourth part describes transport and interaction of electrons, positrons and photons.

For latter three parts, CORSIKA contains several models that maybe activated with varying precisions of the simulations and consumption time of CPU.

### 4.2. Program model options

The hadronic interactions at the high energies may be described by the following six reaction models alternatively

:

- **DPMJET**: DPMJET (Dual Parton Model with JETs) describe high energy hadronic interactions of hadronic-nucleus and nucleus-nucleus collisions using two-component DPM with soft chains and multiple mini-jets at each elementary interaction. Remember to select the DPMJET option when extracting the FORTRAN code from the source file before using DPMJET.
- **EPOS**: EPOS(Energy conserving quantum mechanical multi-scattering approach, based on Partons, Off-shell remnants and Splitting parton ladders) is a improved version of NEXUS ,which uses the universality hypothesis to treat the high energy interactions and combines features of the former VENUS and QGSJET01 with extensions enabling a safe extrapolation up to higher energies.In EPOS, high density effects have been included, and also the screening effects have been simplified using a more phenomenological approach mainly based on the recent RHIC data.For using EPOS you first have to select the EPOS option when extracting the FORTRAN code from the source file.
- **HDPM**: a set of routines to simulate high-energy hadronic interactions produced by Capdevielle [24] and inspired by the Dual Parton Model [26]. These routines are fast and adjusted to experimental data where available. Proton-proton interactions simulated with HDPM and other models agree fairly well with each other. Experimental data are however rare for high energy nucleon-nucleus or nucleus-nucleus collisions and here the results start to disagree due to the simpler modeling in HDPM. As the HDPM routines are default you have nothing to specify when extracting the FORTRAN code from the source file.

- NEXUS: NEXUS (NEXt generation of Unified Scattering approach) extensions of enabling a safe extrapolation up to higher energies based on VENUS and QGSJET, and use the universality hypothesis to treat the high energy interactions. It handles nucleus-nucleus collisions with an up to date theoretical approach. For using NEXUS you first have to select the NEXUS option when extracting the FORTRAN code from the source file.
- QGSJET: QGSJET (Quark Gluon String model with JETs) a quark-gluon-string model using quasi-eikonal Pomeron parametrization for elastic hadron-nucleon scattering amplitude. The hadronization process is treated in the quark gluon string model. For using QGSJET you first have to select the QGSJET or QGSII options when extracting the FORTRAN code from the source file.
- SIBYLL: simulation hadronic interactions at extreme high energies based on QCD mini-jet model. For using SIBYLL you first have to select the SIBYLL option when extracting the FORTRAN code from the source file.
- VENUS: VENUS (Very Energetic NUClear Scattering) to simulate ultra-relativistic heavy ion collisions. For using VENUS you first have to select the VENUS option when extracting the FORTRAN code from the source file.

Hadronic interactions at lower energies are simulated with one of the following models:

- FLUKA: FLUKA (FLUctuating KAscade) a package of routines to follow energetic particles through matter by Monte Carlo method. FLUKA is used within CORSIKA to calculate the inelastic hadron cross-sections with the components of air and to perform their interaction and secondary particle production, including many details of the de-excitation of the target nucleus.
- GHEISHA: GHEISHA (Gamma Hadron Electron Interaction SHower code) a package that has been proven to describe hadronic collisions up to 100 GeV. GHEISHA is used in CORSIKA to calculate the elastic and inelastic cross-sections of hadrons below 80 GeV in air and their interaction and particle production.
- URQMD: UrQMD (Ultra-relativistic Quantum Molecular Dynamics) to treat low energy hadron-nucleus and especially nucleus-nucleus interactions. UrQMD 1.3 cors is used in CORSIKA to perform the elastic and inelastic interactions of hadrons below 80 GeV in air.

The interactions of electrons and photons can be treated with the shower program:

- NKG: formulas to obtain electron densities at selected locations and the total number of electrons at up to 10 observation levels. The longitudinal electron numbers and pseudo-age parameters are calculated every  $100 \text{ g/cm}^2$  above the lowest observation level and the lateral electron densities are calculated for a radial grid of 80 points at the two lowest observation levels.

## 4. Simulation of Air Shower

- EGS4: following each particle and its reaction explicitly. No special option for extracting the FORTRAN code from the source file is required.

Besides the above models, there are several models simulating Cherenkov radiation as well.

- Cherenkov Standard Option : The Cherenkov photons are considered within a wavelength band specified by the upper and lower limits. It records only the photons at the lowest observation level.
- Cherenkov Wavelength Option: the index of refraction is made wavelength dependent in the CERWLEN option.
- Imaging Atmospheric Cherenkov Telescope Option: routines treating the Cherenkov radiation for IACT.
- Imaging Atmospheric Cherenkov Telescope extension Option: extended by parameters describing the emitting particle with the IACTEXT option.
- Cherenkov light reduction option: with the CEFFIC option, light absorption within the atmosphere, telescope mirror reflectivity are taken into account.
- INTCLONG and NOCLONG option: preprocessor option for selecting modes of longitudinal distribution of photons.
- STACEE option: the output of the Cherenkov file is generated in a format used for STACEE experiment.

In principle, most options can be combined. In this thesis, QGSJET option is used, which is an extension of the QGS model[27, 28], which describes hadronic interactions on the basis of exchanging supercritical Pomerons.

More detailed description of CORSIKA program frame, the used cross-sections, the hadronic interaction model HDMP, the electromagnetic interaction models and the particle decays can be found in [25].

### 4.3. Data Files

#### 4.3.1. Input Files

To run a simulation several input files are needed to read. The recent routines need some parametrized data contained within the data files qgsdat-II-03 and sectnu-II-03. (The QGSJET01c routines need some parametrized data contained within the data files QGSDAT01 and SECTNU). They will be generated at the first call within that directory from where you are calling CORSIKA. Later calls will read in these data files qgsdat-II-03 and sectnu-II-03 (resp. QGSDAT01 and SECTNU). These data files are written and read via logical units 1 and 2.

To run a simulation one need to read in several input files. Besides the data files,

CORSIKA needs the input of steering keywords to select the subject and the parameters of the simulation.

The simulation of the air showers is steered by the keywords in the input card image format. An input card example including QGSJET option of CORSIKA can be found in appendix A.

### 4.3.2. Output Files

There are several output files produced by a simulation run. The output files are listed below :

- list file : the control information about the simulation run, the program version with interaction model, steering keywords, physical constants, the atmosphere model and the primary particle.
- file name '*ATnnnnnn*' : this file contains the information about all the particles that reaches the observation level. And it is written onto the output directory DSN. *nnnnnn* means the run number which is specified by the keyword RUNNER.
- file name '*DATnnnnnn.tab*' : this file contains a table of the number of the binned  $\gamma$  's,  $e_{\pm}$  and  $\mu_{\pm}$  particles, and output to the directory DSN. *nnnnnn* means the run number as well. Further details on this file are given in [25].
- file name '*DATnnnnnn.long*' : the longitudinal distribution of particle numbers and energy deposits can be written out to the file, and output to the directory DSN. *nnnnnn* means the run number which is specified by the keyword RUNNER.
- file name *DATnnnnnn.dbase* : to establish a summary file on the contents of an air shower library an optional output file containing a run summary is written to it on the directory DSN. *nnnnnn* is the run number specified in the keyword RUNNR. The name could be '*DATnnnnnn.info*' ,when the AUGERINFO option is used.

All these files are the output of a simulation run using QGSJET option. Some are needed as the input files for the simulation of REAS2, which will be introduced in the next chapter.



## 5. Simulation of Radio Emission

In the last chapter, an air shower generating program is introduced. However, the propagation trajectory of the air shower is still not the directly captured signals by observatory on the ground. Some more simulations should be run to generate effects induced by the air shower. And those effects should include detectable signals. A good C++ code for the simulation which is called Radio Emission from Air Showers (REAS) will be introduced in this chapter.

### 5.1. Geosynchrotron Model

Cherenkov radiation and acceleration of charged particles in the earth magnetic field are the two main emission mechanisms that have been proposed in the past for radio emission from EAS. While the former is dominant in case of dense media, polarisation measurements in a number of experiments subsequently supported the dominance of the geomagnetic emission mechanism for radio emission from EAS in air[29].

Coherent geosynchrotron emission from highly relativistic electron-positron pairs is very attractive because it has been well-understood and also excellent for the development of the emission model. Coherence effects are usually not considered in radio emission from cosmic ray air showers. However, they have to be taken into account under this model.

#### 5.1.1. Synchrotron-theory: individual particles

The acceleration of a charge leads to electromagnetic radiation. Particle motion in the magnetic field can be approximated as an instantaneous circular trajectory with adequate curvature radius. Retardation effects caused by the finite speed of light give rise to strong beaming effects for highly relativistic particles.

The geometry of the problem corresponds to 5.1. If one chooses the origin of the coordinate system to lie in the point on the particle trajectory where the angle between instantaneous particle velocity vector  $\mathbf{v}$  and line of sight vector  $\hat{\mathbf{n}}$  reaches its minimum  $\theta$ .

Define the quantity  $A(R, \omega)$  as a measure of the frequency component  $\omega$  of the electric field normalised to unit solid angle  $\Omega$ . From the view of the 5.2,  $A(R, \omega)$  can be approximated divided into the two perpendicular components  $\hat{e}_\perp$  and  $\hat{e}_\parallel$ . Thus,  $A(R, \omega)$  can be written as

$$A(R, \omega) = \frac{\omega e}{\sqrt{8c\pi}} e^{i(\omega \frac{R}{c} - \frac{\pi}{2})} [-\hat{e}_\parallel A_\parallel(\omega) \pm \hat{e}_\perp A_\perp(\omega)], \quad (5.1)$$

## 5. Simulation of Radio Emission

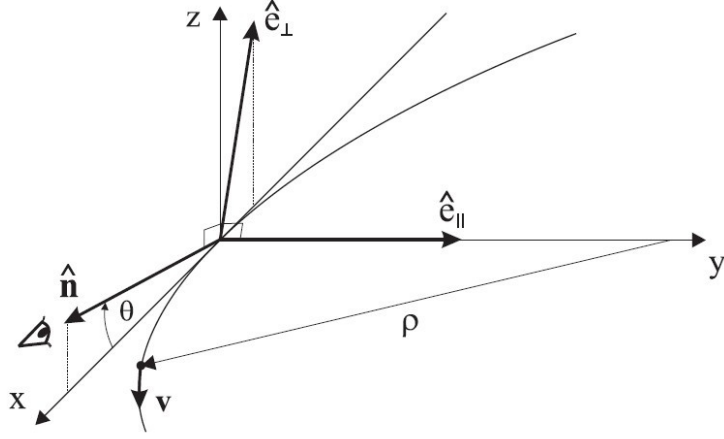


Figure 5.1.: Geometry of single particle synchrotron radiation with particle velocity vector  $\mathbf{v}$ . It is observed with line-of-sight vector  $\hat{\mathbf{n}}$  and enclosed a minimum angle  $\theta$ .  $\rho$  is the equivalent curvature radius.

where the plus-sign is to be used for electrons and the minus-sign for positrons,  $e$  indicates their unit charge. Therefore,

$$A_{\parallel}(\omega) = i \frac{2\rho}{\sqrt{3}c} \left( \frac{1}{\gamma^2} + \theta^2 \right) K_{\frac{2}{3}}(\xi), \quad (5.2)$$

$$A_{\perp}(\omega) = \theta \frac{2\rho}{\sqrt{3}c} \left( \frac{1}{\gamma^2} + \theta^2 \right)^{\frac{1}{2}} K_{\frac{1}{3}}(\xi) \quad (5.3)$$

with

$$\xi = \frac{\omega\rho}{3c} \left( \frac{1}{\gamma^2} + \theta^2 \right)^{\frac{3}{2}}, \quad (5.4)$$

where  $\omega = 2\pi\nu$  denotes the angular frequency corresponding to the observing frequency  $\nu$ ,  $K_a$  denotes the modified Bessel-function of order  $a$ , and the curvature radius of the instantaneous circular orbit is given by

$$\rho = \frac{v\gamma m_e c}{eB \sin \alpha} \quad (5.5)$$

with magnetic field strength  $B$  and pitch angle  $\alpha$  between the particle trajectory and the magnetic field direction.

Since the energy spectrum is  $\propto A(R, \omega)^2$ , it grows as  $N^2$  with particle number  $N$  if

one assumes fully coherent emission. Given a specific distance to the observer  $R$  the frequency component of the E-field can be calculated as

$$E(R, \omega) = \left(\frac{4\pi}{c}\right)^{\frac{1}{2}} \frac{1}{R} A(R, \omega). \quad (5.6)$$

For a given distribution of gyrating particles, the corresponding  $E(R, \omega)$  can then be superposed to calculate the total emission.

### 5.1.2. Synchrotron-theory: electron-positron pairs

Electrons and positrons are created in pairs in the air shower. The symmetry arising from the opposite curvature of electron and positron trajectories can lead to a simplification of the calculation. For an electron-positron pair with perfectly symmetric trajectories with regards to the observer, the  $A_{\parallel}$  contributions from the two particles add up to  $2A_{\parallel}$ . And the  $A_{\perp}$  contributions completely cancel each other.

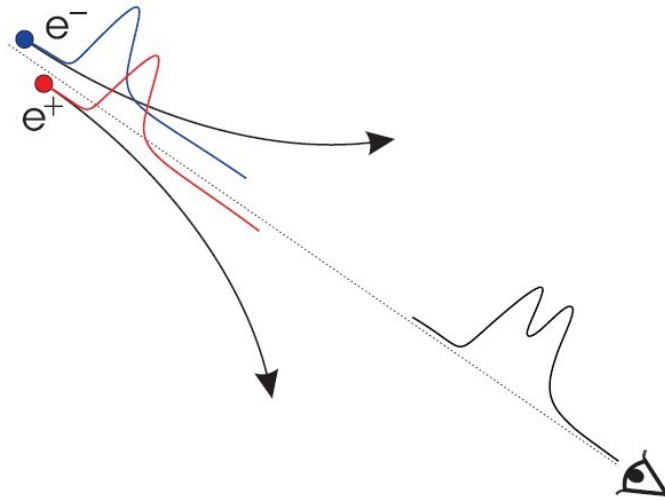


Figure 5.2.: The electron and the positron in an electron-positron pair. Coherent addition of the individual emissions are not allowed.

The direction distribution of the particles instantaneous velocity vectors decides whether a consequent pairing with symmetric trajectories is possible. Then we assume a  $\delta$  - distribution of the particle velocity directions at any given point in the shower shell, as we choose the initial velocity vectors to point radially away from the spherical shower surface. In this situation, the pairing of particles with symmetric trajectories becomes simple as long as one allows pairing between positrons and electrons from generations of particles with a certain net offset in generation time.

## 5. Simulation of Radio Emission

In this scenario of high particle density and  $\delta$  - distribution of velocity directions, the emission from an “effective” electron-positron pair can therefore be approximated as that from a pair with perfectly symmetric trajectories:

$$E_p(R, \omega) \approx \left(\frac{4\pi}{c}\right)^{\frac{1}{2}} \frac{1}{R} \frac{2\omega e}{\sqrt{8c\pi}} e^{i(\omega \frac{R}{c} - \frac{\pi}{2})} (-\hat{e}_{\parallel}) A_{\parallel}(\omega). \quad (5.7)$$

Furthermore it demonstrates that  $A_{\perp}$  is not dominating the emission, and therefore gives further confidence in the approximation.

Effectively, this result allows us to drop the differentiation between positrons and electrons and to consider only generic “particles” hereafter. The spectrum emitted by such an individual particle then corresponds to:

$$E_p(R, \omega) = \left(\frac{4\pi}{c}\right)^{\frac{1}{2}} \frac{1}{R} \frac{\omega e}{\sqrt{8c\pi}} e^{i(\omega \frac{R}{c} - \frac{\pi}{2})} (-\hat{e}_{\parallel}) A_{\parallel}(\omega). \quad (5.8)$$

Superposition of these spectra for all particles in the shower, correctly taking into account the phase differences arising from their relative positions, then yields the emission from the air shower as a whole.

## 5.2. Introduction to REAS

REAS, The C++ code for the simulation of Radio Emission, currently implements the geosynchrotron model. The initial version of the Monte Carlo code, REAS1 calculated radio emission based on parameterised air showers. What will be used here is REAS2, a improved version of REAS1. The current version uses a sophisticated air shower model derived on a shower-to-shower basis from CORSIKA. REAS2 allows an independent selection between parameterisation and histogram for each of the relevant particle distributions, enabling us to study the changes arising from using a more realistic air shower model in detail.

The process of simulating radio emission from extensive air showers can be separated into two steps with REAS2. First, the air shower is simulated as usual with CORSIKA, adopting the desired interaction models and simulation parameters. A tailor-made interface code is used to collect the relevant particle information in histograms during the air shower simulation. At the end of the simulation, based on ROOT data structures, the histograms are saved to disk in a compact data file.

The following particle information is collected for electrons and positrons separately in dozens of slices equidistantly distributed in slant atmospheric depth over the air shower evolution :

- one three-dimensional histogram of
  1. particle arrival time relative to that of an imaginary primary particle propagating with the speed of light from the point of first interaction

2. lateral distance of the particle from the shower core
  3. particle energy
- and one three-dimensional histogram of
    1. angle of the particle momentum to the shower axis
    2. angle of the particle momentum to the (radial) outward direction
    3. particle energy

A four-dimensional distribution of particles in atmospheric depth, arrival time, lateral distance and energy, can be accessed by these histograms, and as well as the angular distribution of particle momenta as a function of particle energy and atmospheric depth. By the way, effects associated with air showers induced by different types of primary particles can be analysed in detail with this simulation strategy.

In a second step, these histograms are imported in the REAS2 code. They are used to recreate particles which follow the given distributions and then calculate the radio emission from the deflection of the particles in the earth magnetic field.

## 5.3. Data Files

### 5.3.1. Input Files

Since REAS2 simulation is based on the result of the CORSIKA simulation, running a corresponding CORSIKA simulation should be the first step. Once the CORSIKA simulation has finished, you will have the following files that are needed for the REAS simulation :

- *RUNxxxxxx.inp* : the CORSIKA steering card file
- *DATxxxxxx.long* : a file with all longitudinal evolution profiles, one per run
- *DATxxxxxx-y.hist* : a number of histogram files, one per shower in the run

Except the CORSIKA output, some configuration files are needed to be set up in order to run the corresponding REAS simulations. The configure files would be :

- *event.reas* : a file setting up the REAS simulation parameters
- *east.grnd* or *all.list* : a file setting up the active observer positions; grnd-files specify observers on a regular grid, whereas list-files specify positions of arbitrarily spaced observers.

A list of the REAS keywords and their meaning will be provided in the example *.reas* parameter file which can be found in appendix B.

## 5. Simulation of Radio Emission

### 5.3.2. Output Files

After a REAS simulation run, several output files are produced. All data are saved as ASCII-text. The file informations are listed below[30]:

- *event.reas* : The input file is written with the values actually used in the simulation run. Values imported from CORSIKA will be written to the corresponding fields in the *.reas* file.
- *event.east.log* : This file contains the copy of the on-screen output of the simulation. Also, you can check which random seed was actually used here if *RandomSeed* is set to be 1.
- *event.efflong* : This holds the longitudinal evolution profile that REAS actually used. (in case of *ShowerType* =1 and *HistogrammedLongitudinalEvolutionToggle* =1).
- *event.east.tracks* : This file contains the fraction of particle trajectories. Blank lines separate the individual trajectories. The columns in the file denote the north, west and height coordinates of each particle as it flies on its trajectory.
- *event.east.bins* : Actually, it is a helper file for data reduction with REASPlot. It lists the data files in the *event east/* directory together with their x, y and z coordinates followed by a quantity describing when the bin has been shut down.
- *event east/*: This is the directory in which the main results (the time-series data for the individual ground bins) are saved.

The *event east/* directory, contains the raw time-series data named *raw\_XXXXm\_YYydeg.dat* file. The columns specify the absolute time step and the north-, west-, and vertical component of the electric field. The raw time-series data represents pulses calculated for infinite bandwidth.

# 6. Simulation Result

## 6.1. Introduction

In the chapter 4 and 5, we described the design and the usage of two simulation codes CORSIKA and REAS2, which are used for air shower and radio emission simulation in the scheme of coherent geosynchrotron radiation. These simulations are based on analytic parametrisations of the air shower characteristics and radio emission characteristics.

In this article, the result inferred from simulations performed with the code will be presented. With a short description of the underlying simulation parameters in section 6.2, detailed characteristics of the radio emission in general will be discussed next. The consumption time will be discussed as the start of the simulation analysis in the section 6.3. We analyse the radial dependence and emission pattern of magnetic field in a qualitative way in the next section. In the next step, shower azimuth angle and polarisation is parametrised by a comparison of the emission from  $10^{19}$  eV airshowers with  $20^\circ$  zenith angle. In the section 6.8, we discuss the symmetry pattern depends on the characters of individual directions. In the end, we conclude the chapter in the last section.

## 6.2. Simulation parameters

All simulations presented here were done with the Monte Carlo code described in chapter 4 and 5. In this section we specify the simulation strategy as well as the parameters and configuration options that were used throughout this work.

We choose  $10^{19}$  eV air shower with  $\theta$  equals  $20^\circ$  as a reference. And change only  $\phi$  from  $0$  to  $315^\circ$  by  $45^\circ$  at a time to analyse its effect on the radio emission. This implies that the effects introduced by changes of the different parameters are well-separable.

The following settings are kept throughout all simulations if not explicitly stated otherwise. The program model of CORSIKA is NEXUS Option in High Energy Hadronic Interaction Model. The magnetic field is chosen with a strength of 0.246 Gauss, which approximately corresponds to the configuration present in Malgou. A total of 160 bins (16 in azimuth; 10 in radius, up to a distance of 500 m) is calculated in each simulation.

## 6.3. Consumption Time

During the simulation run, the time cost of the CORSIKA and REAS2 is about dozens of hours based on the parameters used. The simulation of radio emission from a  $10^{19}$

## 6. Simulation Result

Table 6.1.: The time cost by the simulation of air showers with different energy level. The azimuth angle and zenith angle in CORSIKA are  $0^\circ$ , and the azimuth angle in REAS2 is  $0^\circ$  as well.

Energy (eV)	Totaltime (h:m:s)	CORSIKA (h:m:s)	REAS2 (h:m:s)
$10^{15.5}$	05:38:39	00:07:45	05:30:54
$10^{16}$	06:06:25	00:12:26	05:53:59
$10^{16.5}$	06:06:44	00:17:31	05:49:13
$10^{17}$	05:35:06	00:27:02	05:08:04
$10^{17.5}$	06:45:56	00:42:27	05:03:29
$10^{18}$	06:29:40	01:19:47	05:09:53
$10^{18.5}$	09:08:06	02:37:20	05:30:46
$10^{19}$	11:04:05	05:47:01	05:17:04
$10^{19.5}$	21:04:16	14:10:32	06:53:44
$10^{20}$	41:37:33	36:17:30	05:20:03

eV air shower with 16 azimuth bins and 10 radius bins needs more than 27 hours. Thus, the consumption time is needed to be taken into consideration. In particular, different energy set and more bins on the observation level will cost even more time.

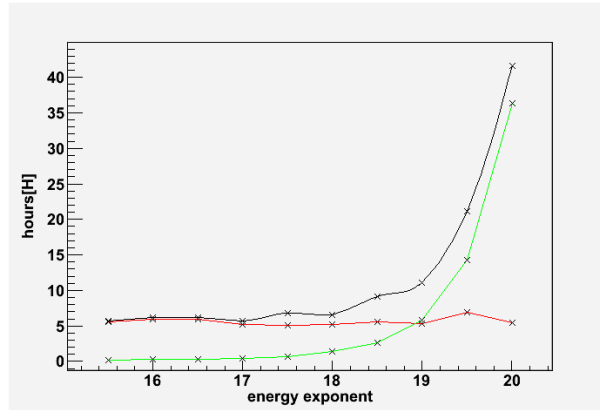


Figure 6.1.: The time cost of simulation with different energies. The azimuth and radius bins are 5 and 10 for each. Black: total time, red: time cost by REAS2, green: time cost by CORSIKA.

First of all, the dependence of the calculation time on the energy is listed in Table 6.1: In this comparison, the azimuth bins and radius bins are chosen to be 5 and 10. From the result, it is obviously that the time cost of REAS2 is not influenced by the variation of the energy. On the other hand, with increasing energy, the time needed by

CORSIKA increases rapidly. It demonstrates that the energy has only an effect on the CORSIKA simulations.

After the energy exponent reaches 17, the time cost by CORSIKA arises rapidly from 27 minutes to 36 hours and 17 minutes. While the energy varies from  $10^{15.5}$  eV to  $10^{20}$  eV, the time cost of REAS2 remains closely around 6 hours. Meanwhile, as we can see in the Fig6.1, the mean time cost of REAS2 is 21591 seconds, which is equivalent to 5.99 hours with a low standard deviation of 603 seconds. That indicates that the data points tend to be very close to the mean. Due to low energy cut-off (in GeV) of the particle kinetic energy are fixed, as the energy level goes up, more particles will be produced and calculated in the air shower, which extend the period correspondingly.

Table 6.2.:

Radial bins	Azimuth bins	Energy (eV)	Totaltime (h:m:s)	CORSIKA (h:m:s)	REAS2 (h:m:s)
10	5	$10^{19}$	11:04:05	05:47:01	05:17:04
10	8	$10^{19}$	14:41:57	05:55:37	08:46:20
10	16	$10^{19}$	27:46:38	05:49:48	21:57:50
20	16	$10^{19}$	39:21:51	05:50:50	33:31:01

For the next step, another essential parameter, the number of simulated antenna positions is studied. As can be seen in table 6.2, the radial bins are chosen from 10 to 20 and azimuth bins from 5 to 16. The difference between the consumption time are obvious.

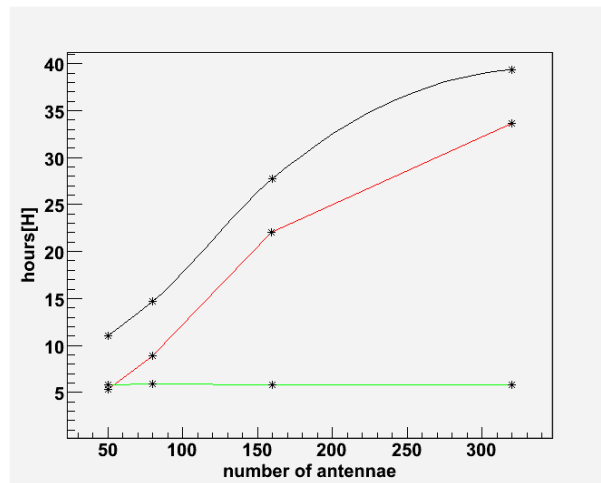


Figure 6.2.: The time cost of the simulation run with different numbers of antenna and a shower energy  $10^{19}$  eV. Black: total time, red: time cost by REAS2, green: time cost by CORSIKA.

## 6. Simulation Result

Since the simulation of the REAS2 are based on the antenna bins, which are supposed to have no relation with CORSIKA. In comparison to the energy variation, the time cost by CORSIKA remains the same for different energies, as shown in Fig 6.2. The variation of time cost depends on the REAS2, due to the increasing antenna numbers. As it is presented, from the general characteristics of radio emission simulation for an air shower of the energy with  $10^{20}$  eV and 320 antenna would be a time costive choice for the simulation run. Thus, we select  $10^{19}$  eV airshower with 160 antenna on the observation level in this work.

### 6.4. Radial dependence and emission pattern

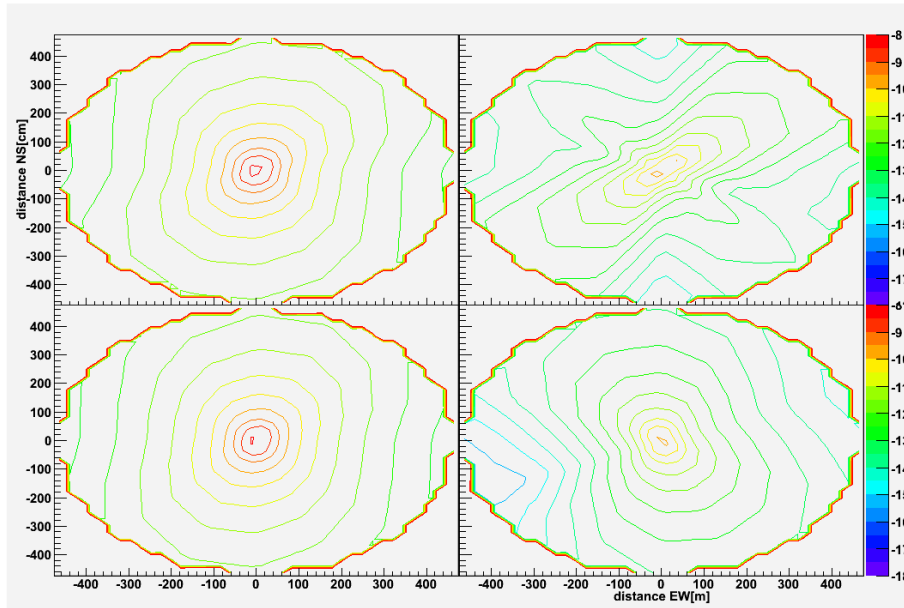


Figure 6.3.: The component of the electric field strength emitted by a air shower with the energy of  $10^{19}$  eV in the individual linear polarisation directions. From top left to bottom right: total field strength, north-south polarisation component, east-west polarisation component, vertical polarisation component. The x-y axis stands for various distance to the shower core. The values in z axis are electric field strength in logarithm scale.

Fig 6.3 shows the component of the electric field strength in the individual linear polarisation directions north-south, east-west and vertical. The total field strength pattern is remarkably symmetric in spite of the intrinsic asymmetry of the geomagnetic emission mechanism.

Fig 6.4 depicts the relation between the individual polarisation component and the total electric field strength. The total field strength is almost coincided with the field strength on east-west direction. It illustrates that the east-west component dominates

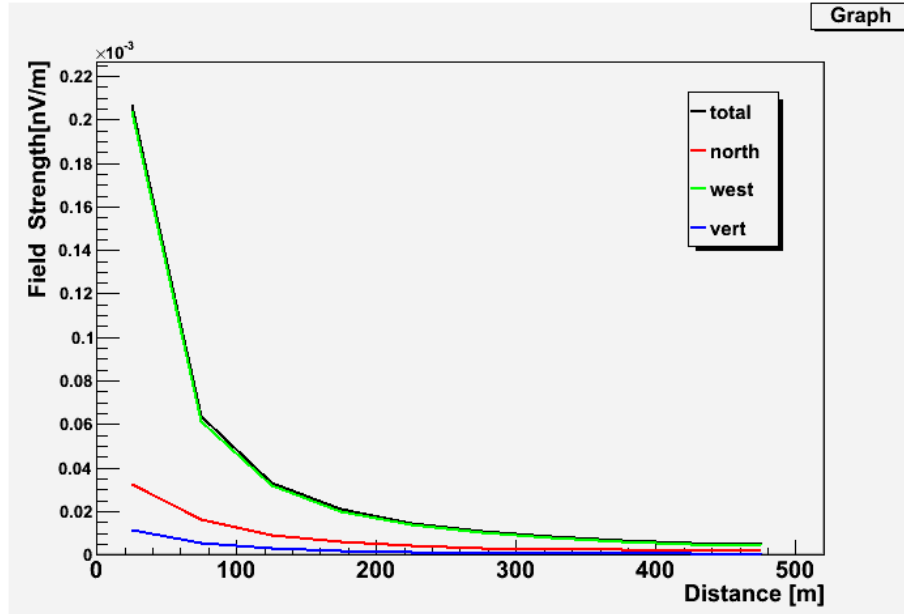


Figure 6.4.: The component of the electric field strength emitted by a air shower with  $10^{19}$  eV in the individual linear polarisation directions with  $45^\circ$  azimuth angle and  $20^\circ$  angle. Black: total field strength, red: north-south component, green: east-west component, blue: vertical component. The x axis stands for various distance to the shower core.

the three individual linear polarisation directions.

Note that we can equivalently use the east-west polarisation component or the total field strength in many of the following analyses as there is no flux in the north-south (let alone vertical) polarisation component along the north-south direction from the shower centre for air showers coming from the south.

In Fig 6.5, we compare the east-west polarisation component at the positions of 75 meters away from the observation center.

## 6.5. Zenith dependence and emission pattern

The Fig 6.6 indicates the contour plots of the emission from a  $10^{19}$  eV air shower with  $45^\circ$  azimuth angle as a function of shower zenith angle. The total field strength pattern is elongated due to the projection effects arising at high shower zenith angles. The patterns are much more circular, but retain a significant intrinsic ellipticity and asymmetry. By increasing the zenith angle, the field strength rises as well. We can see from the three columns of Fig 6.6 that the field strength in the different zenith angles has a direct dependence on the geomagnetic field distribution. The signal is gently going from the

## 6. Simulation Result

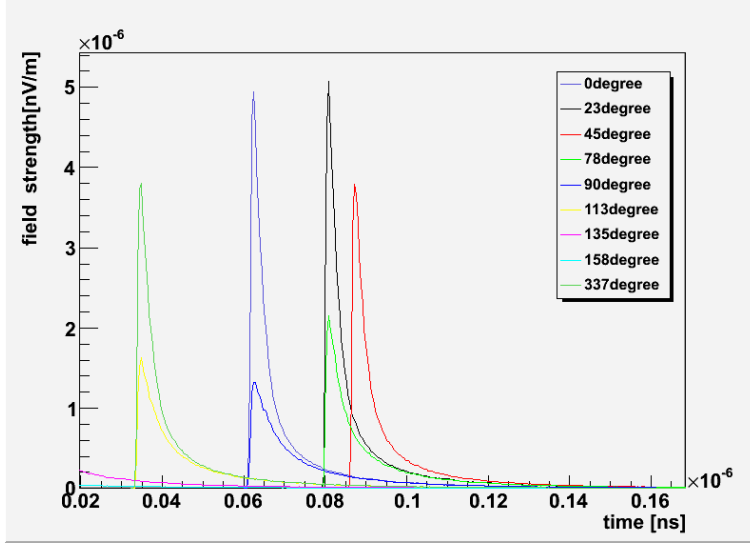


Figure 6.5.: The log field strength on east-west component at the positions of 75 meters away from the observation center with different azimuth angle of antenna position listed. The energy of the primary particle of the air shower is  $10^{19}$  eV, while the zenith angle is  $20^\circ$  and the azimuth angle is  $45^\circ$ . The plot is mirror symmetry by  $45^\circ$  azimuth angle as well as  $225^\circ$ . Time starts with the first shower occurring.

central regions to high zenith degree emission.

However, though difference of the distribution exist, we can not distinguish the zenith angle because of the similarity. Due to the zenith dependence of the distribution characteristics, experiments which measure the zenith characteristics of the emission can not directly verify the geomagnetic origin of the radio emission from cosmic ray air showers.

### 6.6. Shower azimuth angle

An important feature of the radio emission is its predicted polarisation, which is directly related to the shower azimuth angle. Knowledge of this dependence is imperative for the planning and interpretation of experimental measurements.

A comparison of the emission from  $10^{19}$  eV airshowers with  $20^\circ$  zenith angle as a function of azimuth angle of CORSIKA can be seen in Fig 6.7, with the REAS2 azimuth angle with  $45^\circ$ . Due to the projection effects arising at high shower azimuth angles in CORSIKA, the total field strength pattern is rotated.

The total field strength pattern of the emission (left column) simply rotates as a function of azimuth angle in CORSIKA. In other words, no significant information associated to the geomagnetic field direction is present in the signal. As a direct consequence, it is

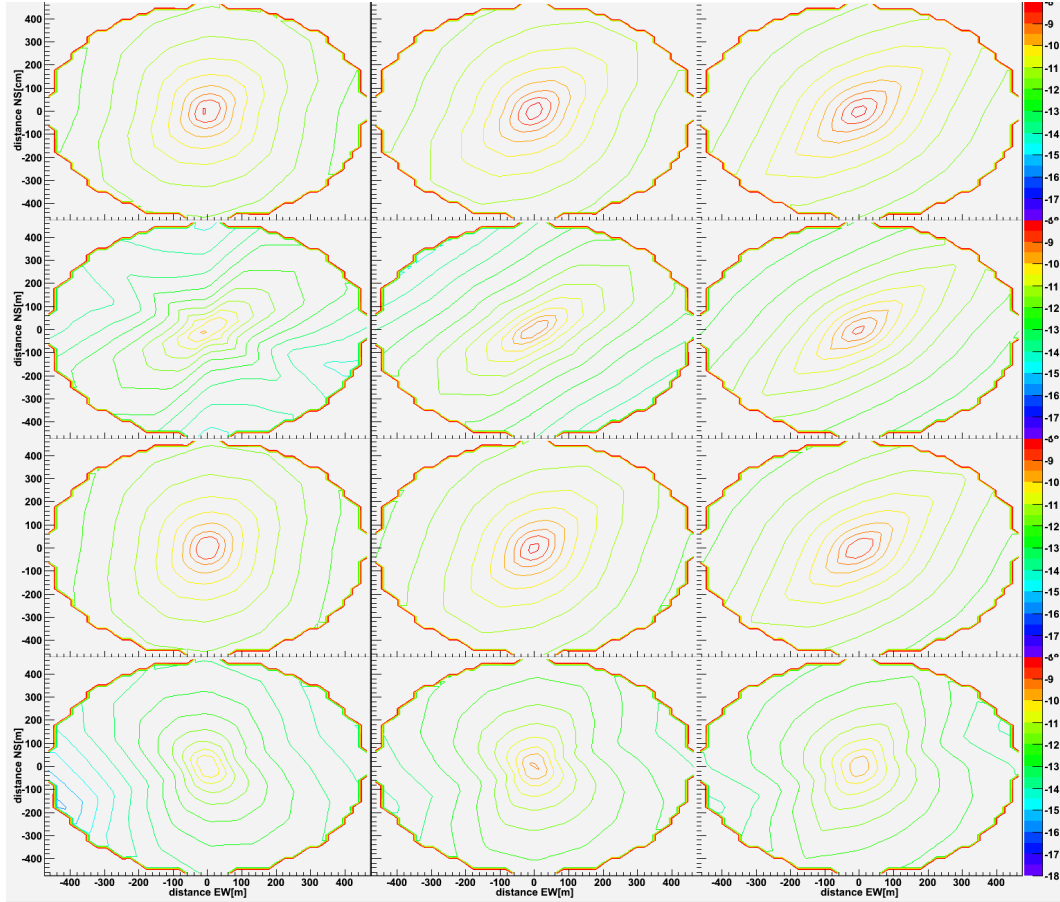


Figure 6.6.: Contour plots of the emission for  $10^{19}$  eV air shower with  $45^\circ$  azimuth angle as a function of distance to the shower core for various zenith angles. Columns from left to right:  $20^\circ$ ,  $40^\circ$  and  $60^\circ$  zenith angle. Lines from top to bottom: total field strength, north-south, east-west and vertical polarisation component. The x and y axis stands for various distance to the shower core on east-west and north-south respectively. The values in z axis are electric field strength in logarithm scale.

## 6. Simulation Result

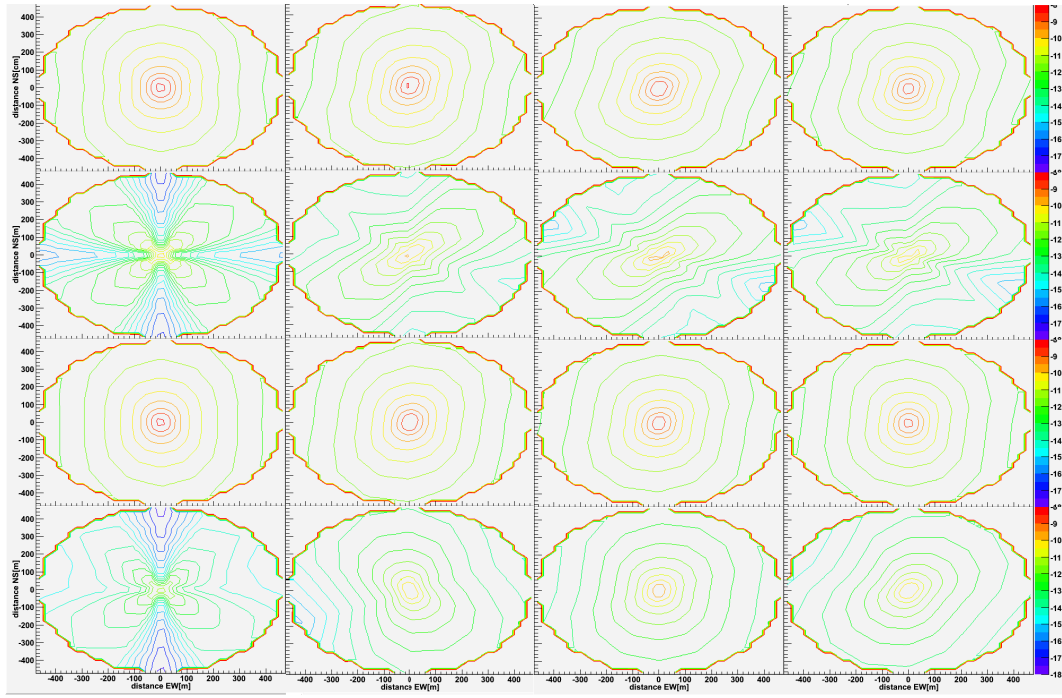


Figure 6.7.: Contour plots of the emission for  $10^{19}$  eV air shower with  $20^\circ$  zenith angle as a function of distance to the shower core for various azimuth angles. Columns from left to right:  $0^\circ$ ,  $45^\circ$ ,  $90^\circ$  and  $135^\circ$  azimuth angle for CORSIKA. The azimuth angle  $\phi$  for REAS2 remains as  $45^\circ$ . For lines from top to bottom: total field strength, north-south, east-west and vertical polarisation component. The x-y axis stands for various distance to the shower core. The values in z axis are electric field strength in logarithm scale.

not possible to verify the geomagnetic origin of the emission with an experiment measuring only the total field strength (or only one circular polarisation component) of the emission.

What's more, because the air showers arrive from one azimuthal direction, azimuthal dependence of the measured pulse amplitudes can be seen in statistical samples of measured total field strength pulses. As it is shown in Fig6.4, the east-west component dominates in the three individual linear polarisation directions. Thus, the total field strength have the shape similar to the east-west component.

The situation is obvious when one looks at the individual linear polarisation components. It is visible from the right three columns of Fig6.7 that the field strength in the different polarisation directions has a direct dependence on the geomagnetic field direction: the signal is linearly polarised mainly in the direction perpendicular to the air shower and magnetic field axes, at least in the central regions of high emission.

The relative fullwidth can give another sight to the influence of the CORSIKA azimuth angles. The relative fullwidth  $X$  is defined as:

$$X = \frac{MAX(A(\phi_{CORSIKA})) - MIN(A(\phi_{CORSIKA}))}{(MAX(A(\phi_{CORSIKA})) + MIN(A(\phi_{CORSIKA}))) / 2} \quad (6.1)$$

The  $MAX(A(\phi_{CORSIKA}))$  stands for the maximum of the field strength at the antenna studied for different CORSIKA azimuth angles  $\phi$ . Similarly,  $MIN(A(\phi_{CORSIKA}))$  represents the minimum of the field strength for different CORSIKA azimuth angles  $\phi$ . According to the equation, the relative fullwidth of the zenith angle  $20^\circ$  and 8 different azimuth angles for CORSIKA and with  $45^\circ$  REAS2  $\phi$  will be revealed in Fig6.8.

The smallest values, which are between 0.2 and 0.3, lie at the antenna nearest to the shower core. While the relative fullwidth gets larger as the antenna goes far from the shower core, until it reaches the edge with the value of 0.935. It can be inferred that, the field strength remained stable in the center part with high values comparatively, while it drops off in the border with a changeable value.

An other important feature caused by the changing REAS2 azimuth angles with the same CORSIKA azimuth angle and zenith angle is what we are interested in. The dependence of the REAS2  $\phi$  on the field strength on antenna can be seen in Fig6.9. The distribution of field strength on total vector and three orientations rotates in the function of REAS2 azimuth angles  $\phi$ . As a consequence, the emitted radiation pattern have a mirror symmetry with regard to  $180^\circ$  of the REAS2 azimuth angle.

The relative fullwidth also illustrates the information of dependence on the REAS2 azimuth angles. Comparing the Fig 6.8 and Fig6.10, the shape is similar with each other. But the latter holds the value between 0.45 and 0.85, which indicates the relative fullwidth becoming more stable in the function of REAS azimuth angle  $\phi$ .

## 6. Simulation Result

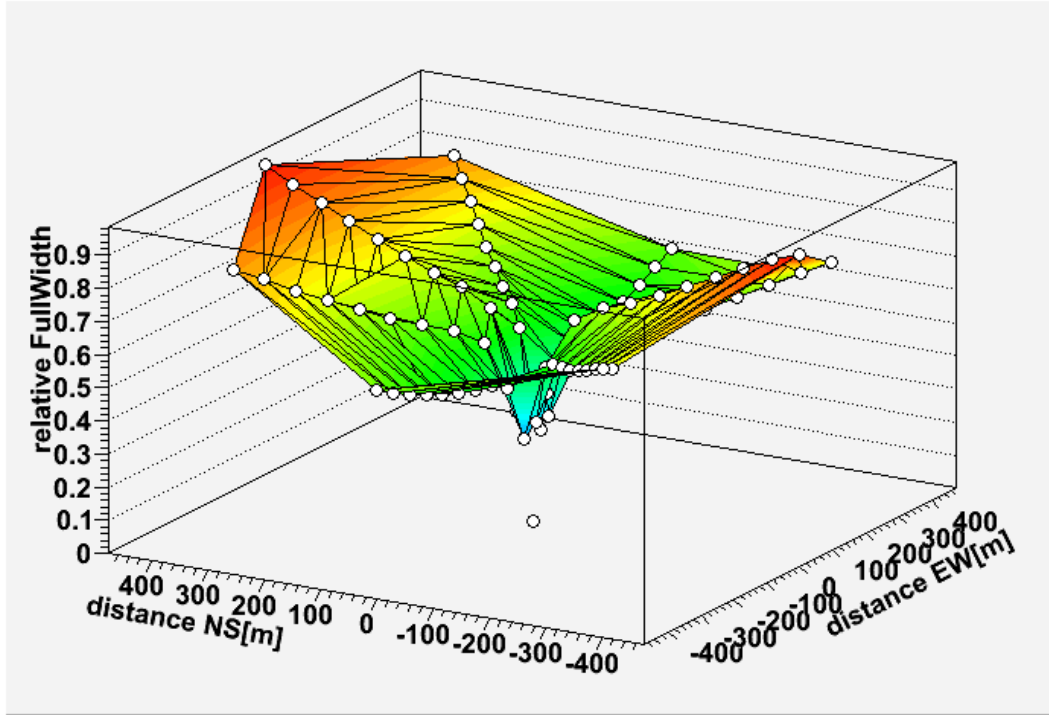


Figure 6.8.: Relative Fullwidth of the total field strength based on zenith angle  $20^\circ$  and 8 different azimuth angles for CORSIKA and with  $45^\circ$  azimuth angle in REAS2. The emission from  $10^{19}$  eV airshowers with  $20^\circ$  zenith angle influence on the 80 antenna(10 radial and 8 azimuth).

### 6.7. Maxium/Integral ratio

The electric field strength on the antenna is influenced by the emitted radiation produced by air showers. In Fig6.11, shows the way field strength goes based on time and on different distance to the center core. It takes the  $20^\circ$  zenith angle and  $45^\circ$  azimuth angle for CORSIKA by a  $10^{19}$  eV air shower in this case, with  $45^\circ$  azimuth angle  $\phi$  for REAS2. The reduction of Pulse height happens as it get away from the center core of the observer antenna.

There are two methods in common use to check the field strength on the antenna, which are the integral value and the maximum value. Therefore, we consider how the maximum value dominates in the integral of the total field strength. That is what represents in the Fig6.12. Obviously, from the figure, the ratio reaches its maximum at the distance of 25 meters, since the nearest antenna to the shower center. Also, there exists fluctuation of the ratio based on the angles, the minimum at  $90^\circ$  and  $270^\circ$ . However, at the outermost antenna of 475 meters, the ratio develop into 0.02 with no angle influence on it any more.

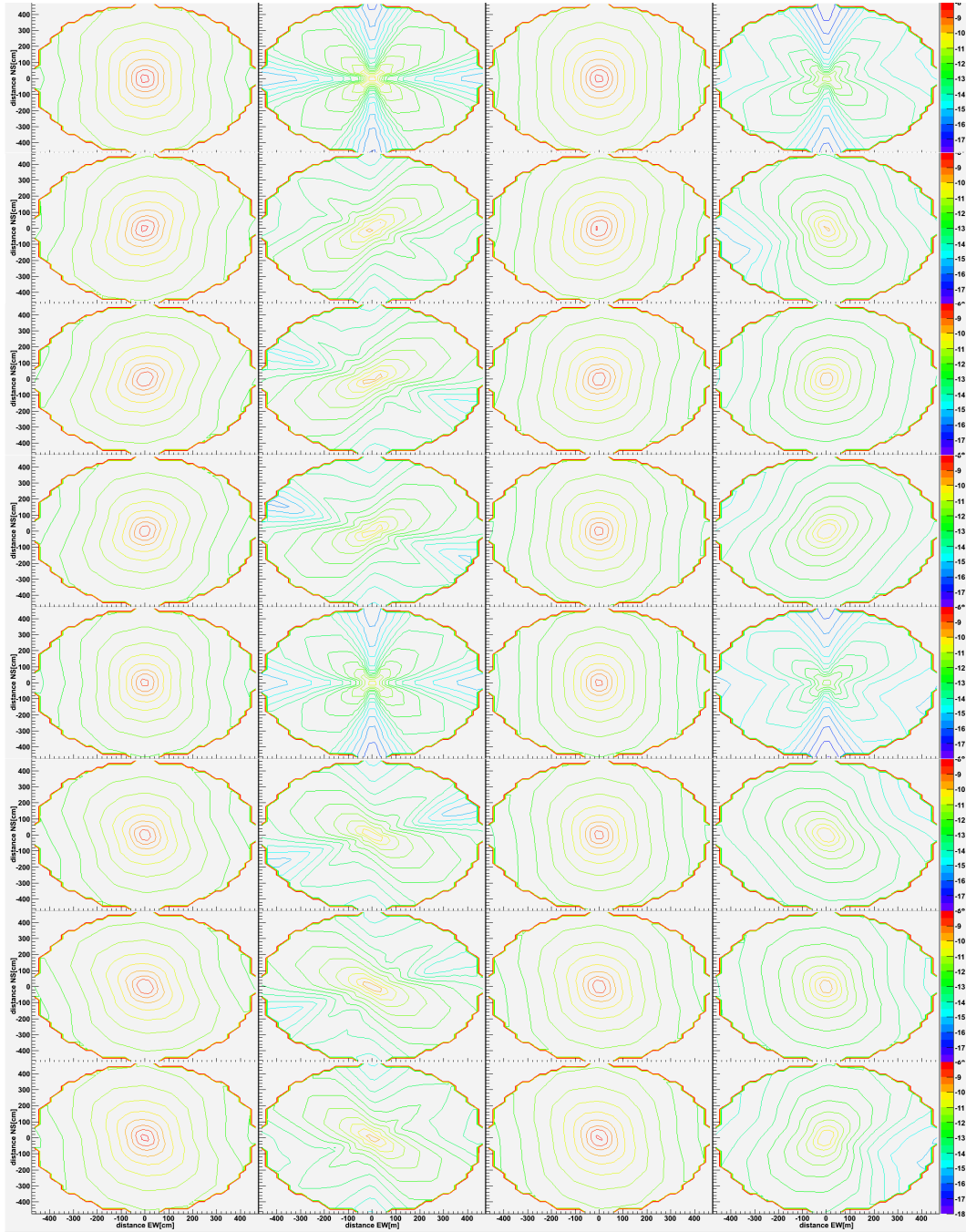


Figure 6.9.: Contour plots of the emission from a  $10^{19}$  eV air shower with  $20^\circ$  zenith angle as a function of distance to the shower core to various azimuth angles in REAS2. Columns from left to right: total field strength, north-south, east-west and vertical polarisation component. The azimuth angle  $\phi$  for CORSIKA maintains as  $45^\circ$ . For lines from top to bottom:  $0^\circ$ ,  $45^\circ$ ,  $90^\circ$ ,  $135^\circ$ ,  $180^\circ$ ,  $225^\circ$ ,  $270^\circ$  and  $315^\circ$  azimuth angle for REAS2. The x-y axis stands for various distance to the shower core. The values in z axis are electric field strength in logarithm scale.

## 6. Simulation Result

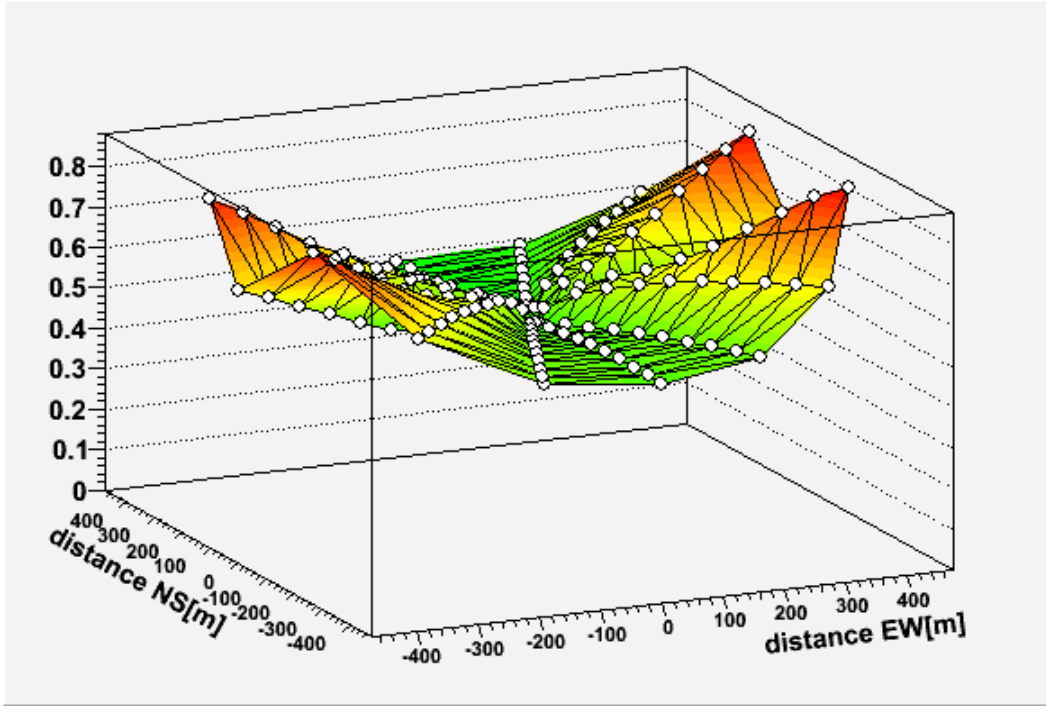


Figure 6.10.: Relative Fullwidth of the total field strength of  $20^\circ$  zenith angle and  $45^\circ$  azimuth angles for CORSIKA and with different azimuth angle in REAS2. The emission from  $10^{19}$  eV airshowers with  $20^\circ$  zenith angle influence on the 160 antenna(10 radial and 16 azimuth).

### 6.8. Symmetry N-S and E-W

For a vertical air shower, the emitted radiation pattern must have a number of inherent symmetries. In particular, the east and west directions are completely equivalent so that the emission pattern must be symmetric in east and west. For a electric field, north and south must also be equal.

In our simulation with the zenith angle  $\theta = 20^\circ$ , the symmetry in east and west directions are changed. Assume that  $A$  stand for the electric field strength of position on the observer level. And  $x(\phi, R)$  represents the electric field strength in the certain region with  $\phi$  between  $0^\circ$  and  $180^\circ$ . By the law of point symmetry, the relation of  $A$  with different intervals of antenna azimuth angle in  $0^\circ < \phi < 360^\circ$  is:

$$A = \begin{cases} x(\phi, R) & : 0^\circ < \phi < 180^\circ \\ x(\phi - 180^\circ, R) & : 180^\circ < \phi < 360^\circ \end{cases}$$

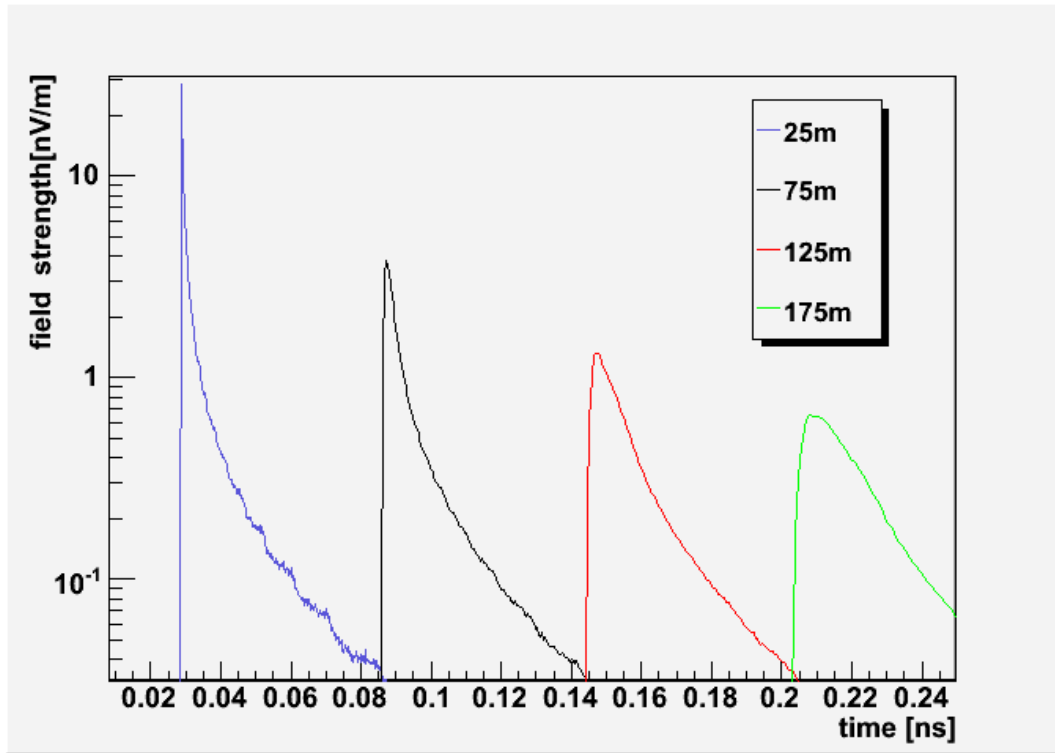


Figure 6.11.: Log total Field strength on the antenna of the emission from a  $10^{19}$  eV air shower as a function of time to various distance to the shower center. With  $20^\circ$  zenith angle and  $45^\circ$  azimuth angle for CORSIKA. The azimuth angle  $\phi$  for REAS2 maintains as  $45^\circ$ . Distance to the shower center, blue: 25 meters, black: 75 meters, red: 125 meters, green: 175 meters.

where  $\phi$  is the azimuth angel on the observation level.

Obviously, the situation of nonvertical showershower is much more complex. When the CORSIKA azimuth angle  $\phi$  comes to  $45^\circ$ ,  $90^\circ$  or else, the symmetry of the emitted radiation pattern will alter as well. This is obviously very different from the vertical air shower induced radio emission.

As can be seen in Fig 6.7, the symmetry pattern of north component, which in the second column, the the field strength with primary particle energy are shown. And one detailed example is Fig 6.13. There is a significant dependence of the emission on the shower zenith angle. Additionally, it is one of the parameters that undergoes strong fluctuations between individual showers with otherwise identical parameters. It is therefore interesting to evaluate the dependence of the emission on this parameter.

The value of the magnetic field strength on three directions can be calculated from just

## 6. Simulation Result

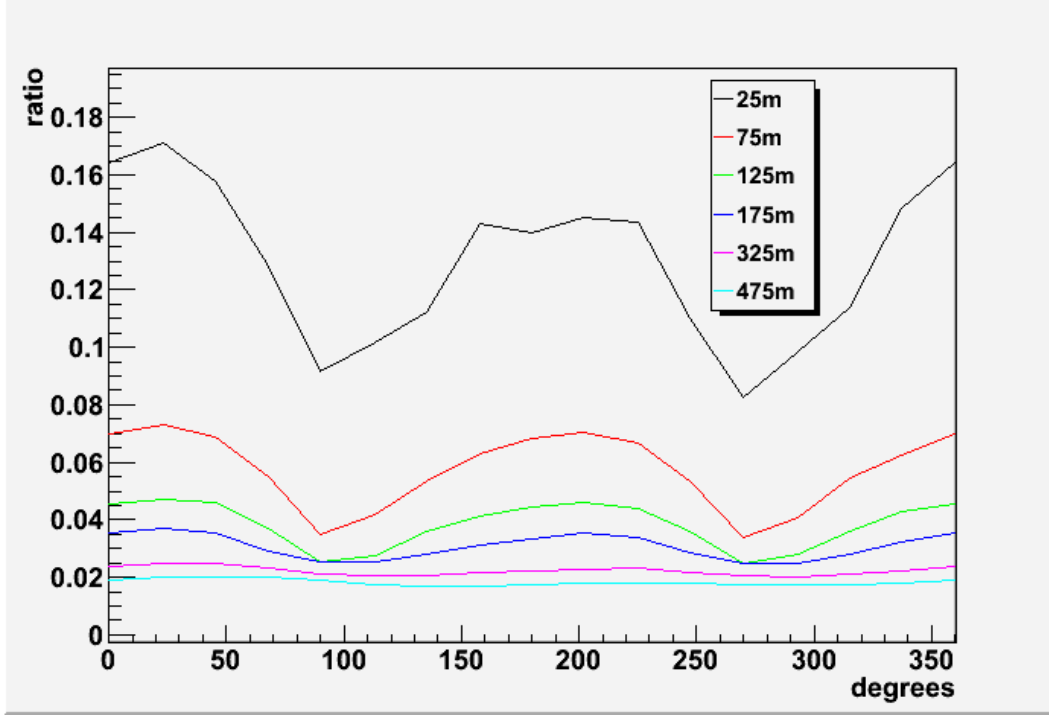


Figure 6.12.: The maximum/integral ratio as a function of degrees with different distance to the shower core. With emission from a  $10^{19}$  eV air shower,  $20^\circ$  zenith angle and  $45^\circ$  azimuth angle for CORSIKA and  $45^\circ$  azimuth angle for REAS2. Distance to the shower center, black: 25 meters, red: 75 meters, green: 125 meters, blue: 175 meters, pink: 325 meters, cyan: 475 meters.

one quarter part (antenna angle  $\phi$  between  $45^\circ$  and  $135^\circ$ ):

$$A = \begin{cases} x(\phi, R) & : 45^\circ < \phi < 135^\circ \\ x(270^\circ - \phi, R) & : 135^\circ < \phi < 225^\circ \\ x(\phi - 180^\circ) & : 225^\circ < \phi < 315^\circ \\ x(90^\circ - \phi, R) & : -45^\circ < \phi < 45^\circ \end{cases}$$

Moreover, for the different REAS2 azimuth angles of fixed azimuth and zenith angles in CORSIKA, the symmetry still holds. For instance, Fig6.9 with Contour plots of the emission from a  $10^{19}$  eV air shower with  $20^\circ$  zenith angle as a function of distance to the shower core to various azimuth angles in REAS2. In other words, this equation works for all the situation. The fact that these intrinsic symmetries are fulfilled as expected provides an important consistency check. Furthermore, one can use these symmetries to save computation time by calculating only a half or even quarter-plane on the ground

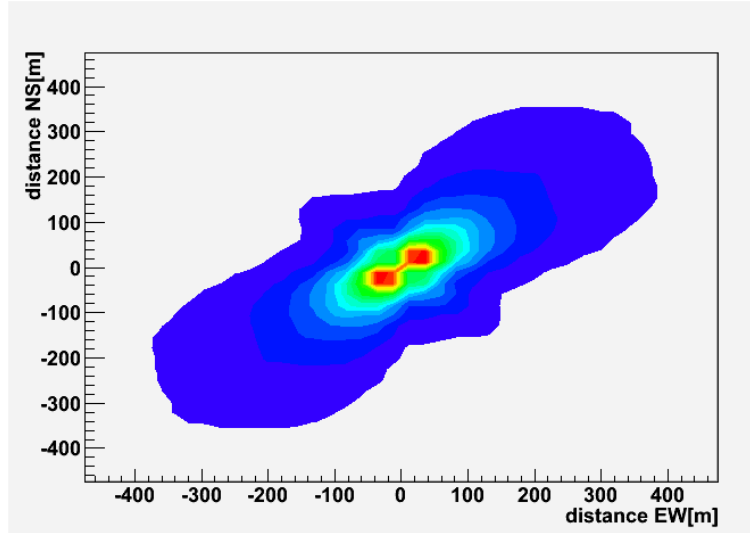


Figure 6.13.: An example to show the symmetry pattern of the north-south component emitted from a  $10^{19}$  air shower with  $20^\circ$  zenith angle and  $45^\circ$  azimuth angle in CORSIKA. The x-y axis stands for various distance to the shower core.

and then mirroring the results accordingly. The raw data which can prove the symmetry can be seen in Appendix C.

## 6.9. Conclusions

The major result of this work is the analysis of the characteristics of the emission generated in the geomagnetic emission scenario. The overall symmetries in the emission pattern can make experimental setups measuring only the total field strength and particular component much easier. Also, time cost dependence of energy and antenna would be taken into consideration for users to run corresponding simulations efficient.

Another result of the simulation is the effects arising in air showers with different azimuth angles in CORISKA with same azimuth angle in REAS2 and different azimuth angles in REAS2 with same azimuth angle in CORISKA. The emission pattern associated to the increasing azimuth angles both in CORISKA and REAS2 influence with projection effects. And it makes inclined air showers an interesting target for simulation.

The other results of the simulation, radial depend and emission pattern, especially the symmetry pattern which could be useful in the simulation for geosynchrotron emission are some topics for interpretation of concrete experiments.



## 7. Summary and Outlook

We have performed a detailed analysis of radio emission from cosmic ray air showers in the scheme of coherent geosynchrotron radiation. The properties of the radiation generated by the geomagnetic emission mechanism have been established.

Firstly, in this work, CORSIKA simulation run used to generate extensive air shower with  $10^{19}$  eV. Afterwards, import the results from CORSIKA into REAS2 to produce radio emissions. The analysis of the characteristic of the radio emissions generated in the geomagnetic emission scenario is the major result. we have then performed extensive simulations of air showers in order to establish the radio emissions dependence on the air shower geometry and specific air shower parameters such as the primary particle energy, the polarisation of the air shower and the magnetic field configuration. Major results are the dependence of radial, shower azimuth, zenith angle and emission patterns. We have a qualitative discussion of these and other important effects. Besides, we also have successfully incorporated the analysed dependences into an overall parametrisation. This Coherent geosynchrotron emission model makes it easier for the comparison of experimental data. Furthermore, it allows to relate important air shower parameters directly to specific characteristics of the radio emission. The parametrisation summarises the cumulative modelling effort performed in this thesis. And it is a very useful tool for the study of radio emission from cosmic ray air showers.

The advances in the theoretical modelling of the emission come out. And also for upcoming results from experimental projects such as LOPES, radio emission from cosmic ray air showers thus has made great advances on the way towards being established as an additional observing technique for cosmic ray research. Since only a few parameters are investigated in this work, much more simulations are still need to be done. The research on this effective way should meet the general requirements of qualified air shower characteristic analysis.



## 8. Acknowledgement

At the very first, I want to thank Prof. K.-H. Kampert who gave me the opportunity to work in this exciting experiment with the support of a large and active group. I am also extremely grateful to Dr. Julian Rautenberg for many constructive discussion and help in all issues even in very busy times. I appreciate the very welcoming and friendly atmosphere of the Astroparticle Group in Wuppertal when continuing my research in Germany. I want to express my gratitude to all members of this group for fruitful discussions and backing throughout of this work. Special thanks to Prof. Markus Risse for good advice. Thanks to my office mates Pietro Oliva and Andreas Schwarz for their patience. Furthermore, I would like to thank He Xi for answering my questions and encourage.

In the end I want to express my gratitude to my friends and family who always supported me during my studies with patience and encouragement.



## A. Input Card Example

RUNNR	1	run number
EVTNR	1	number of first shower event
NSHOW	1	number of showers to generate
PRMPAR	14	particle type of prim. particle
ESLOPE	-2.7	slope of primary energy spectrum
ERANGE	10E7 10E8	energy range of primary particle in GeV
THETAP	0. 10.	range of zenith angle (degree)
PHIP	45 45	range of azimuth angle (degree)
SEED	1 0 0	seed for 1. random number sequence
SEED	2 0 0	seed for 2. random number sequence
OBSLEV	145200	observation level (in cm)
FIXCHI	0.	starting altitude (g/cm**2)
MAGNET	20.1 -14.2	magnetic field at Malrgue, centr. Europe 20.0 42.8
HADFLG	0 0 0 0 0 2	flags hadr.interact.&fragmentation
ECUTS	0.3 0.3 0.000401 0.000401	energy cuts for particles
MUADDI	T	additional info for muons
MUMULT	T	muon multiple scattering angle
ELMFLG	T T	em. interaction flags (NKG,EGS)
STEPFC	1.0	mult. scattering step length fact.
RADNKG	200.E2	outer radius for NKG lat.dens.distr.
ARRANG	0.	rotation of array to north
LONGI	T 5. T T	longit.distr. & step size
fit	out	
ECTMAP	25000	cut on gamma factor for printout
MAXPRT	100	max. number of printed events
DIRECT	./data/	output directory
DATBAS	T	write .dbase file
USER	you	user
DEBUG	F 6 F 1000000	debug flag and log.unit for out
PAROUT	T T	#
RADNKG	500000	#
THIN	1e-06 10000 30000	#
THINH	1 100	#
EXIT		terminates input



## B. REAS Parameter File Example

### # global parameters:

ParameterFileVersion = 20 ; do not change manually  
NumParticlesToCalculate = 1000000000  
NumSimultaneousParticles = 100000  
RandomSeed = -1 ; -1: chosen randomly, other: chosen manually  
TrajectoryMonitoringFraction = 0.0001  
AtmosphereModel = 0 ; 0: US Standard, 10: Argentina Winter,  
20: Europe January, 30: South Pole March,  
90: Constant Density

### # parameters setting up the spatial observer configuration:

ObserverType = 0 ; 0: regular grid (grnd-file), 1: antenna list (list-file)  
ObserverHeight = 0 ; in cm, for antenna lists this will be averaged  
from antenna heights  
MaximumRadius = 50000; in cm, only for regular grid  
NumAzimuthalBins = 8 ; only for regular grid  
NumRadialBins = 10 ; only for regular grid  
CoreShiftToNorth = 0 ; in cm, only for antenna list, in plane of  
averaged antenna heights  
CoreShiftToWest = 0 ; in cm, only for antenna list, in plane of  
averaged antenna heights

### # parameters setting up the temporal observer configuration:

TimeLowerBoundary = -1 ; in s, only if AutomaticTimeBoundaries set to 0  
TimeUpperBoundary = 1 ; in s, only if AutomaticTimeBoundaries set to 0  
InnerTimeAlgorithm = 3 ; 2: SimpleGrid, 3: ClassicGrid  
InnerTimeResolution = 2e-10 ; in s  
OuterTimeResolution = 2e-10 ; in s, is set to InnerTimeResolution for ClassicGrid  
ReductionToOuterTimeGridToggle = 0 ; is deactivated for ClassicGrid  
GroundLevelRefractiveIndex = 1 ; specify refractive index at 0 m asl

### # parameters setting the optimisation strategies:



**# parameters specific to CORSIKA based showers - other parameters are read from the CORSIKA input file:**

CorsikaFilePath = data/ ;	path to the CORSIKA files
CorsikaParameterFile = input-card ;	specify CORSIKA card file
CorsikaSlantOptionToggle = 0 ;	set to 1 if CORSIKA option SLANT is used
SelectedCorsikaShower = 1 ;	0: averaged, i: i-th shower
UseCorsikaAzimuthToggle = 1 ;	0: use azimuth angle provided above, 1: use CORSIKA provided azimuth
HistogrammedShowerEvolutionToggle = 1 ;	if 0, evolution is parametrised
HistogrammedLateralDistributionToggle = 1 ;	if 0, lateral distribution is NKG
HistogrammedLongitudinalDistributionToggle = 1 ;	if 0, longitudinal distribution is Gamma-pdf
HistogrammedParticleEnergiesToggle = 1 ;	if 0, energy distribution is parametrised as set above
HistogrammedPitchAngleDistributionToggle = 1 ;	if 0, spherical surface with 2300 m radius
PairWiseCreation = 2 ;	0: always paired, 1: ratio paired (histogrammed distribs.), 2: never paired (histogrammed evolution)
ShowerEvolutionShift = 135 ;	apply slant depth shift to CORSIKA-derived shower evolution, in g/cm ** 2

**# parameters related to electric field effects:**

ElectricFieldToggle = 0 ;	enabling turns off gamma-cone-cutting!
ElectricFieldStrength = 100 ;	in V/m
ElectricFieldInclinationAngle = 90 ;	in degrees, 90: field points downwards
ElectricFieldAzimuthAngle = 0 ;	in degrees, 90: field points westwards



## C. Example of raw data from REAS2

Table C.1.: North component of the electric field. Azimuth degrees from  $0^\circ$  to  $270^\circ$ .

Radial Position	$0^\circ$	$90^\circ$	$180^\circ$	$270^\circ$
1	2.9808e-05	3.56844e-05	2.93833e-05	3.52194e-05
2	7.65739e-06	1.07733e-05	7.86431e-06	1.05226e-05
3	3.79285e-06	5.59883e-06	3.88726e-06	5.31715e-06
4	2.33799e-06	3.51702e-06	2.36261e-06	3.29102e-06
5	1.57555e-06	2.44715e-06	1.57768e-06	2.25485e-06
6	1.11187e-06	1.81793e-06	1.12463e-06	1.6446e-06
7	8.29803e-07	1.40124e-06	8.29914e-07	1.24836e-06
8	6.32567e-07	1.11674e-06	6.29364e-07	9.79746e-07
9	4.95967e-07	9.12402e-07	4.97832e-07	7.89594e-07
10	3.95838e-07	7.59681e-07	3.89859e-07	6.515e-07

C. Example of raw data from REAS2

[h]

Table C.2.: North component of the electric field. Azimuth degrees from 45° and 225°.

Radial Position	45°	225°
1	6.81673e-05	6.81356e-05
2	2.72505e-05	2.71091e-05
3	1.48502e-05	1.4806e-05
4	9.60223e-06	9.55145e-06
5	6.89028e-06	6.84016e-06
6	5.27567e-06	5.23884e-06
7	4.21577e-06	4.18784e-06
8	3.47349e-06	3.46452e-06
9	2.92944e-06	2.92913e-06
10	2.5123e-06	2.51594e-06

Table C.3.: North component of the electric field. Azimuth degrees from 135° and 315°.

Radial Position	135°	315°
1	3.03124e-05	3.01855e-05
2	1.13845e-05	1.143e-05
3	5.4585e-06	5.57554e-06
4	3.07275e-06	3.23181e-06
5	2.04948e-06	2.20735e-06
6	1.55503e-06	1.70619e-06
7	1.32228e-06	1.42754e-06
8	1.15957e-06	1.25387e-06
9	1.04203e-06	1.11564e-06
10	9.41468e-07	1.00509e-06

# Bibliography

- [1] A. M. Hillas. *Cosmic rays*. The Commonwealth and International Library. Selected Readings in Physics. Oxford: Pergamon Press, 1972.
- [2] V. F. Hess. *Phys. Z.* 13, 1804 (1912).
- [3] J. Linsley. “Evidence for a primary cosmic-ray particle with energy  $10^{20}$ eV.” *Phys.Rev. Lett* 10. (Feb, 1963) 146C148.
- [4] D. J. Bird et al. “Evidence for correlated changes in the spectrum and composition of cosmic rays at extremely high energies.” *Phys. Rev. Lett.* 71 (Nov, 1993) 3401C3404.
- [5] M. Nagano et al. “Energy spectrum of primary cosmic rays above 1017 ev determined from extensive air shower experiments at akeno.” *Journal of Physics G: Nuclear and Particle Physics* 18 (1992), no. 2, 423C442.
- [6] R. U. Abbasi for the HiRes collaboration. “Observation of the ankle and evidence for a high-energy break in the cosmic ray spectrum.” *Phys. Lett. B*619 (2005) 271C280, astro-ph/0501317.
- [7] V. S. Berezhinsky and S. I. Grigoreva, “A bump in the ultrahigh-energy cosmic ray spectrum.” *Astron. Astrophys.* 199 (1988) 1C12.
- [8] R. Aloisio, V. Berezhinsky, P. Blasi, and S. Ostapchenko. “Signatures of the transition from galactic to extragalactic cosmic rays.” *ArXiv e-prints* 706 (June, 2007)0706.2834.
- [9] A. M. Hillas. The origin of ultra-high-energy cosmic rays. *Ann. Rev. Astron. Astrophys.* 22:425c444, 1984.
- [10] P. Auger, P. Ehrenfest, R. Maze, J. Daudin, and A. F. Robley. “Extensive cosmic-ray showers.” *Rev. Mod. Phys.* 11 (1939) 288C291.
- [11] W. Heitler. *Quantum theory of radiation*. International Series of Monographs on Physics, Oxford: Clarendon, 1954, 3rd ed.
- [12] T. Yamamoto for the Pierre Auger Collaboration. “The uhecr spectrum measured at the pierre auger observatory and its astrophysical implications. Proceedings of the 30th International Cosmic Ray Conference,” 2007.
- [13] J. W. Cronin, T. K. Gaisser, and S. P. Swordy. “Cosmic rays at energy frontier.” *Scientific American* (1997).

## Bibliography

- [14] T. K. Gaisser and T. Stanev. “High-energy cosmic rays.” *Nuclear Physics A* 777 (Oct., 2006) 98C110, astro-ph/0510321.
- [15] J. R. Horandel, “The composition of cosmic rays at the knee.” *Nuovo Cimento B Serie 120* (June, 2005) 825C+, astro-ph/0407554.
- [16] A. M. Hillas. The origin of ultra-high-energy cosmic rays. *Ann. Rev. Astron. Astrophys.* 22:425C444, 1984.
- [17] D. Harari, S. Mollerach, and E. Roulet. “The toes of the ultra high energy cosmic ray spectrum.” *Journal of High Energy Physics* 8(Aug., 1999) 22C+, ArXiv:astro-ph/9906309.
- [18] Heiko Geenen. “Reconstruction of the Primary Energy Spectrum from Fluorescence Telescope Data of the Pierre Auger Observatory.” Doctoral thesis.
- [19] F. Schmidt. Corsika shower images. <http://www.ast.leeds.ac.uk/fs/showerimages.html>
- [20] <http://teachers.web.cern.ch/teachers/archiv/HST2000/teaching/expt/muons/casfig8.gif>
- [21] <http://www-ik.fzk.de/corsika/> Updated 09.Nov, 2009.
- [22] Joel Achenbach (March 2008). “The God Particle”. *National Geographic Magazine*. <http://ngm.nationalgeographic.com/2008/03/god-particle/achenbach-text>. Retrieved 2008-02-25.
- [23] T. Antoni et al.(KASCADE Collaboration), *Nucl.Instr.Meth.A*513(2003)490.
- [24] J. N. Capdeielle, *J. Phys.G:Nucl. Part. Phys.* 15,909(1989).
- [25] D. Heck, T. Pierog. *Extensive Air shower simulation with CORSIKA:a user guide*,Forschungszentrum Karlsruhe GmbH, Karlsruhe.
- [26] A. Capella and J. Tran Thanh Van. *Phys. Lett. B*93 (1980) 146
- [27] A. B. Kaidalov and K. A. Ter-Martirosyan, *Sov. J. Nucl. Phys.* 39 (1984) 979
- [28] A. B. Kaidalov, K. A. Ter-Martirosyan and Yu. M. Shabelsky, *Sov. J. Nucl. Phys.*43 (1986) 822
- [29] Buniy Ralston 2002; Zas et al. 1992; Alvarez-Müniz et al. 2000
- [30] T. Huege, “REAS 2.59 Users Manual”, 2008, Karlsruhe.